Epigenetic therapy targets the 3D epigenome in endocrine-resistant breast cancer

Authors:

Joanna Achinger-Kawecka[1,2,11], Clare Stirzaker[1,2,11], Neil Portman[2,3], Elyssa Campbell[1], Kee-Ming Chia[3], Qian Du[1,2], Geraldine Laven-Law[4], Shalima S. Nair[1], Aliza Yong[3], Ashleigh Wilkinson[3], Samuel Clifton[1], Heloise H. Milioli[2,3], Sarah Alexandrou[6], C. Elizabeth Caldon[2,6], Jenny Song[1], Amanda Khoury[1,2], Braydon Meyer[1,2], Julia M.W. Gee[5], Anthony Schmitt[7], Emily S. Wong[8,9], Theresa E. Hickey[4], Elgene Lim[2,3], Susan J. Clark[1,2,10]

[1]Epigenetics Research Laboratory, Cellular Science Pillar, The Garvan Institute of Medical Research, Sydney, New South Wales, Australia
[2]St Vincent's Clinical School, UNSW Sydney, New South Wales, Australia
[3]Connie Johnson Breast Cancer Research Laboratory, The Garvan Institute of Medical Research, Sydney, New South Wales, Australia
[4]Dame Roma Mitchell Cancer Research Laboratories, Adelaide Medical School, University of Adelaide, Adelaide, South Australia, Australia
[5]Breast Cancer Molecular Pharmacology Group, School of Pharmacy and Pharmaceutical Sciences, Cardiff University, Wales, CF10 3NB, UK
[6]Invasion and Metastasis Laboratory, The Garvan Institute of Medical Research, Sydney, New South Wales, Australia
[7]Arima Genomics, Inc., San Diego, California, USA
[8]Victor Chang Cardiac Institute, Sydney, New South Wales, Australia
[9]School of Biotechnology and Biomolecular Sciences, UNSW Sydney, New South Wales, Australia
[10]Lead Contact
[11]These authors contributed equally

Correspondence

s.clark@garvan.org.au (S.J.C.)

j.achinger@garvan.org.au (J.A-K.)

Keywords

3D genome architecture; DNA methylation; Decitabine, Hi-C; epigenetic therapy; ER+ breast cancer; endocrine-resistance; transcription factors; enhancers

Abstract

Three-dimensional (3D) epigenome remodelling is an important mechanism of gene deregulation in cancer. However, its potential as a target to overcome therapy resistance remains largely unaddressed.

Here we show that FDA-approved epigenetic therapy Decitabine (5-Aza-mC) suppresses tumour growth in preclinical metastatic ER+ breast tumour xenograft models. Decitabine-induced genome-wide DNA hypomethylation results in large-scale 3D epigenome deregulation, including de-compaction of higher order chromatin structure and loss of topologically associated domain boundary insulation. Significant DNA hypomethylation at ER-enhancer elements was associated with gain in ER binding, creation of ectopic 3D enhancer-promoter interactions and concordant activation of ER-mediated transcription pathways. Importantly long-term withdrawal of epigenetic therapy partially restores methylation at ER-enhancer elements, resulting in loss of ectopic 3D enhancer-promoter interactions and associated gene repression.

Our study illustrates how epigenetic therapy has potential to target ER+ endocrine-resistant breast cancer by DNA methylation-dependent rewiring of 3D chromatin interactions associated with suppression of tumour growth.

54 **Main**

55 Around 70% of breast cancers are driven by the Estrogen Receptor-alpha (ER). ER is
56 a critical ligand-activated transcription factor that controls breast cancer cell
57 proliferation and tumour growth upon exposure to estrogenic hormones[1]. Drugs that
58 target ER pathways are highly effective in the treatment of ER+ breast cancer[2,3],
59 however *de novo* or acquired resistance to these agents (endocrine resistance) affects a
60 large proportion (>30%) of patients and is the major cause of breast cancer mortality.
61 Endocrine resistance has previously been shown to be associated with epigenetic
62 alterations, including DNA methylation, chromatin accessibility, histone modifications
63 and binding of different transcription factors[4,5]. In particular, differential ER
64 transcription factor binding leads to altered expression of estrogen-responsive genes in
65 endocrine-resistant breast cancer[1] and is associated with clinical response to endocrine
66 therapies[6,7].

67

68 Epigenetic alterations also influence the three-dimensional (3D) genome architecture,
69 from the local level of chromatin interactions to the higher level organisation of
70 topological associated domains (TADs) and chromosome compartments[8]. Alterations
71 to the 3D genome architecture have been described in a number of different cancers,
72 including prostate cancer[9,10], breast cancer[11-15], gliomas[16], and several hematologic
73 cancers[17,18]. Although cancer cells maintain the general pattern of 3D genome folding,
74 distinctive structural changes have been described in cancer genomes at all of levels of
75 3D organisation[19]. We and others recently reported that 3D genome structure is also
76 disrupted in endocrine-resistant ER+ breast cancer cells[14,15,20], notably through long-
77 range chromatin changes at ER-enhancer binding sites that are DNA hypermethylated
78 in resistant cells[14].

79

80 DNA demethylating agents such as Decitabine (5-aza-2'-deoxycytidine, DAC) have
81 emerged as a promising therapeutic strategy for treating various cancers[21]. Decitabine
82 is approved by many international regulatory agencies, including the US FDA and the
83 European Commission (EC), for treating haematological cancers[21]. In solid cancers
84 (including colorectal and ovarian cancer), Decitabine has been shown to demethylate
85 regulatory regions that result in re-activation of tumour suppressor genes[22,23].
86 Additionally, treatment with DNA de-methylating agents has been shown to stimulate
87 immune response pathways in cancer cells through increased transcription of DNA

88 repeat elements, which induces a viral mimicry response[24-26]. However, the direct effect
89 of these epigenetic drugs on the tumour cells, including epigenome and 3D genome
90 structure, remains largely unexplored, especially in clinically relevant patient-derived
91 model systems or clinical samples.
92
93 To elucidate the mechanism of epigenetic therapy with Decitabine, we assessed the
94 molecular consequences of treatment on DNA methylation, 3D genome architecture
95 and transcriptional programs in endocrine-resistant ER+ patient-derived xenograft
96 (PDX) models. Our data revealed that Decitabine treatment inhibited tumour growth
97 and resulted in DNA hypomethylation that was associated with 3D epigenome
98 remodelling, gain in ER binding and activation of ER-mediated transcription,
99 highlighting the potential of epigenetic therapy in treatment of ER+ endocrine-resistant
100 breast cancer.

Results

Low-dose Decitabine inhibits tumour growth and decreases cell proliferation

To study the efficacy of epigenetic therapy in the context of endocrine-resistant ER+ breast cancer and to establish its impact on the 3D genome and epigenome, we used two different patient-derived xenograft (PDX) models (Gar15-13, HCI-005) (Fig. 1a) (see Methods). Gar15-13 and HCI-005 PDXs were derived from the metastases of ER+ patients who had disease progression following one or more lines of endocrine therapy and have been used for several pre-clinical studies[27-31].

Using a low, well-tolerated and non-cytotoxic dose (0.5mg/kg; Extended Data Fig. 1a) of Decitabine, we first interrogated the anti-cancer effect of epigenetic therapy on tumour growth. Following tumour implantation and initial period of growth (to a volume of 150-200 mm^3), mice were randomized to twice-weekly injections of PBS (Vehicle) or 0.5mg/kg Decitabine. Treatment continued with twice-weekly measurement of tumour volume for 35 days or until tumour volume exceeded 1000 mm^3. At endpoint mice were sacrificed and tumour material collected for analysis. In both Gar15-13 and HCI-005 PDX models, Decitabine treatment elicited a strong growth inhibitory response (Fig. 1b, c) and a significant reduction in the proliferative index as measured by Ki-67 positivity at endpoint (Fig. 1d).

Decitabine induces widespread DNA hypomethylation

To directly identify the epigenetic reprogramming events induced by Decitabine treatment, we first analysed genome-wide DNA methylation data generated using Infinium EPIC Methylation arrays. EPIC arrays were performed on four biological replicates of Vehicle and Decitabine-treated PDX tumours at end-point. All Decitabine-treated tumours exhibited genome-wide DNA methylation loss (Fig. 1e and Extended Data Fig. 1b, c, P value < 0.0001, two-tailed Mann-Whitney test), with Gar15-13 showing more hypomethylation compared to HCI-005 (Fig. 1e and Extended Data Fig. 1d) (average methylation difference 14.55% and 8.74%, respectively). To quantify the extent of DNA methylation loss, we identified differentially methylated probes (DMPs) and differentially methylated regions (DMRs) between Vehicle and Decitabine-treated Gar15-13 and HCI-005 tumours (Supplementary Table 1). Hypomethylated DMPs in both PDX models were mainly located at non-coding genomic regions (introns and

135 intergenic) (Extended Data Fig. 1e, f) and significantly enriched at putative enhancer
136 regions (Fig. 1f and Extended Data Fig. 1g) ($P < 0.001$, permutation test). In agreement,
137 we observed extensive DNA hypomethylation at enhancers in Gar15-13 tumours
138 (approx. 18.38% change in median DNA methylation; Extended Data Fig. 1h, P value
139 < 0.0001, two-tailed Mann-Whitney test) and HCI-005 tumours (approx. 9.24% change
140 in median DNA methylation; Extended Data Fig. 1i, P value < 0.0001, two-tailed
141 Mann-Whitney test), while promoters were less demethylated (approx. 10.12% in
142 Gar15-13 and 2.16% in HCI-005; Extended Data Fig. 1j-k, P value < 0.0001, two-tailed
143 Mann-Whitney test).
144
145 We next evaluated genome-wide DNA methylation levels at different classes of
146 transposable elements (TEs) using the REMP package[32], including LTRs, LINE1
147 elements and Alu elements. We observed genome-wide loss of DNA methylation at all
148 repeat element sub-groups (Extended Data Fig. 1l and Extended Data Fig. 1m) with
149 ~12% loss of DNA methylation in Decitabine treated tumours. Additionally, we
150 observed TE expression alterations and activation of anti-viral signalling
151 (Supplementary Note), as previously observed with Decitabine treatment in other
152 cancers[24,25]. Notably, although all TE classes showed some degree of DNA methylation
153 loss, the extent of DNA hypomethylation measured at repeat elements was less than
154 those observed genome-wide and significantly less compared to DNA hypomethylation
155 at enhancer regions (Extended Data Fig. 1h-i).
156
157 **Loss of DNA methylation results in de-compaction of 3D genome architecture and**
158 **alters TAD boundary insulation**
159 Distinctive structural changes have been described in cancer genomes at all levels of
160 3D organisation[19]. We were therefore motivated to study if Decitabine-induced
161 genome-wide DNA hypomethylation also leads to global changes in 3D genome
162 architecture. We analysed *in situ* Hi-C data (see Supplementary Note) corresponding to
163 three biological replicates of Vehicle and Decitabine-treated tumours in Gar15-13
164 PDX. First, to detect open (active) and closed (silent) genomic compartments (A and
165 B, respectively) we performed PCA analysis of the Hi-C data as described[33].
166 Comparison of eigenvalues between samples revealed differences between Vehicle and
167 Decitabine tumours as shown by reduced correlation (Extended Data Fig. 2a). To
168 further understand these differences, we directly compared the eigenvalues between

169 Vehicle and Decitabine-treated tumours and observed that while most bins retained the
170 same compartment status between the samples (either A to A or B to B), a large number
171 of bins became more A-type in Decitabine as compared to Vehicle (B to A switch) (Fig.
172 2a). We next quantified this switching (see Methods) and identified 643 compartments
173 (i.e. 2.28% of all compartments) that switched their assignment between A and B
174 (Extended Data Fig. 2b). Around 64% of the changes induced by Decitabine involved
175 compartment activation (B-type to A-type) (Fig. 2b). Notably, we observed significant
176 DNA hypomethylation at B to A switches, while A to B switching regions maintained
177 similar DNA methylation levels to Vehicle samples (Fig. 2c). In agreement with B-
178 compartments becoming more de-methylated and active with Decitabine, using RNA-
179 seq data (see Supplementary Table 4) we detected an overall increase in expression of
180 genes located at regions that switched their assignment from B to A in Decitabine-
181 treated tumours, while genes located at A to B switching compartments did not
182 significantly change expression (Extended Data Fig. 2c). The newly activated
183 compartments hosted 21 genes that decreased in expression and 87 genes that increased
184 in expression with Decitabine (Extended Data Fig. 2d, e). Furthermore, we quantified
185 A–A and B–B interaction frequencies in Decitabine and Vehicle-treated tumours and
186 found decreased interaction strength between closed compartments (B-B interactions;
187 $P = 0.025$, two-tailed Students t-test), increased contacts between active compartments
188 (A-A interactions; $P = 0.26$, two-tailed Students t-test) and increased contacts between
189 A-B compartments ($P = 0.011$, two-tailed Students t-test) (Fig. 2d, e and Extended
190 Data Fig. 2f, g).
191
192 We next investigated the impact of Decitabine treatment on the organisation of
193 topologically associated domains (TADs). We observed a significant decrease in the
194 average insulation score in Decitabine as compared to Vehicle-treated tumours (~36.53
195 in Decitabine and ~46.74 in Vehicle) (Fig. 2f and Extended Data Fig. 2h, P value <
196 0.0001, two-tailed Mann-Whitney test), suggesting that loss of DNA methylation is
197 associated with reduced segmentation into TADs. Consistent with loss of TAD
198 boundaries and potential merging of TADs, the total number of TADs was decreased
199 in Decitabine-treated samples (Fig. 2g) and their corresponding average domain size
200 increased (Extended Data Fig. 2i; $P = 0.0289$, t-test). Analysis of differential TAD
201 boundaries revealed a large percentage (43.2%) of Vehicle-specific boundaries, which
202 were lost in Decitabine tumours (Fig. 2h) and characterised by decreased average

203 insulation score in Decitabine tumours (Extended Data Fig. 2j). We exemplify one such
204 region, where a TAD was lost in Decitabine-treated tumours, concomitant with loss of
205 boundary insulation (Fig. 2i; further examples in Extended Data Fig. 2k-l).
206
207 Together, these results indicate that DNA hypomethylation induced by Decitabine
208 treatment *in vivo* leads to significant de-compaction of 3D chromatin architecture, with
209 reduced B-type compartments, increased interactions within A-type compartments and
210 concomitant increase in regional gene expression. While most TADs maintain their
211 structure after Decitabine treatment, their boundaries become less insulated suggesting
212 increased intra-tumour heterogeneity in TAD structure and loss of some TAD
213 boundaries at the regions of chromosomal compartment de-compaction.
214
215 **Loss of DNA methylation results in rewiring of 3D enhancer-promoter**
216 **interactions**
217 Since we observed altered higher-level 3D genome structure and significant
218 hypomethylation at enhancer elements with Decitabine treatment (Extended Data Fig.
219 1h), we next asked if there were alterations in finer-scale 3D chromatin interactions. To
220 gain insights into chromatin interactions at the level of individual promoters and
221 enhancers, we investigated genome-wide promoter-anchored contacts in three
222 Decitabine and three Vehicle-treated tumours using Promoter Capture Hi-C (PCHi-C)
223 (Supplementary Note). Hi-C libraries were hybridised to custom-designed genomic
224 restriction fragments covering 23,711 annotated gene promoters, achieving a clear
225 increase in the coverage of promoter-anchored interactions as compared to Hi-C (Fig.
226 3a). To identify statistically significant interactions between promoters and other
227 regulatory elements from the PCHi-C data, we used the CHiCAGO pipeline[34].
228 Promoter (bait) regions were significantly enriched for active promoters, poised
229 promoters and active enhancers ChromHMM states in both Vehicle and Decitabine-
230 treated tumours (Fig. 3b). Notably, putative enhancer other-end interacting regions (i.e.
231 enhancer OEs; exemplified in Fig. 3a) showed significant differential enrichment,
232 whereby active promoters were enriched in Vehicle tumours and enhancers were
233 enriched in Decitabine-treated tumours, especially active enhancers (Fig. 3b).
234
235 In order to directly identify differential promoter-anchored interactions, we integrated
236 the results generated using Chicdiff[35] pipeline with methods to intersect the promoter

237 bait and enhancer OE regions for each interaction (see Methods). In total, we found
238 13,088 stable (no change) and 4,111 dynamic (gained or lost) contacts for promoters
239 and 55,186 stable and 26,912 dynamic contacts for enhancer OEs (Fig. 3c). The
240 majority of promoter regions were common between the Decitabine and Vehicle
241 tumours. However, Decitabine treatment resulted in a large gain in the number of
242 dynamic enhancer OEs, while only a small number of enhancer OEs were lost (24,694
243 gained and 2,218 lost in Decitabine) (Fig. 3c). Notably, interactions at gained enhancer
244 OEs with Decitabine treatment were associated with longer interaction distances as
245 compared to these that were at maintained or lost (Fig. 3d), consistent with an increased
246 number of long-range interacting enhancers connecting to these promoters.
247
248 We next compared the total number of unique promoter and enhancer OE regions
249 involved in interactions between Vehicle and Decitabine-treated tumours and found a
250 significant increase in the number of enhancer OEs in Decitabine tumours while the
251 number of interacting promoters stayed the same (Extended Data Fig. 3a, b). On
252 average we detected 3.73 unique enhancer OEs per promoter in Vehicle samples and
253 7.06 unique enhancer OEs per promoter in Decitabine samples (Fig. 3e). To directly
254 assess the gain in the number of interacting enhancers with Decitabine, we calculated
255 the number of interacting enhancer OEs per each individual promoter and compared
256 this number between Vehicle and Decitabine-treated tumours (Fig. 3f). We found that
257 the majority of bait promoters involved in interactions in Vehicle tumours showed a
258 large gain in the number of enhancer OEs they connect to in Decitabine-treated
259 tumours, suggesting reprogramming of one-to-many enhancer-promoter interactions.
260 Furthermore, we identified gained multi-way interactions that had, on average,
261 significantly higher CHiCAGO scores in Decitabine-treated tumours compared to
262 Vehicle (Wilcoxon P value < 0.0001) (Extended Data Fig. 3c), consistent with an
263 overall increase in the total number of interactions with Decitabine treatment.
264
265 Given that the frequency of interactions is directly linked with higher-order
266 compartment assignment, we next measured the overlap between dynamic promoter-
267 anchored interactions and A/B compartment flipping. We found that the gain of
268 interactions was associated with a shift from B compartment assignment toward
269 compartment A in Decitabine-treated tumours (~76%) (Fig. 3g and Extended Data Fig.
270 3d), while a loss of interactions was associated with switch from A-type to B-type

271 assignment (~80%). This was particularly pronounced at lost interactions involving
272 promoter bait regions (>90% switched A to B) (Fig. 3g).
273
274 Together, these results support that 3D chromatin interactions are rewired following
275 Decitabine-induced DNA methylation loss, leading to increased promoter-anchored
276 interactions involving multiple enhancers connecting to gene promoters.
277
278 **Rewiring of 3D chromatin interactions aligns with altered transcription and gain**
279 **in ER binding at ER-mediated enhancers**
280 To examine the transcriptional consequences of Decitabine-induced rewiring of 3D
281 chromatin interactions, we next analysed RNA-seq data corresponding to four
282 replicates of Decitabine-treated and Vehicle Gar15-13 PDX tumours. Gene set
283 enrichment analysis (GSEA)[36] of all differentially expressed genes revealed that
284 Decitabine treatment negatively correlated with gene signatures of cell proliferation
285 and cell cycle (E2F targets, G2M checkpoint and Myc targets; for example *SMC3*, *TK1*
286 and *KIF20A*) (Fig. 4a), consistent with supressed tumour growth and decreased
287 cytological proliferation markers observed (Fig. 1d), as well as genes involved in viral
288 mimicry response (see Supplementary Note), as described previously[25]. Surprisingly,
289 Decitabine treatment also enriched for multiple hallmark genesets related to hormone
290 signalling (estrogen response early and estrogen response late) (Fig. 4a) and up-
291 regulation of a significant proportion of genes belonging to the Hallmark Estrogen
292 Response genesets (Extended Data Fig. 4a).
293
294 To directly address if rewired enhancer-promoter interactions are involved in altered
295 transcription, we identified genes connected to newly gained enhancer OEs and
296 compared their average expression between Vehicle and Decitabine tumours. We
297 identified a total of 4025 genes at new enhancer-promoter interactions (Supplementary
298 Table 6), of which 417 were upregulated after Decitabine treatment (P value < 0.05;
299 logFC > 1) (Fig. 4b). Upregulated genes were significantly enriched at gained OE
300 interactions as compared to all genes (Fisher's exact test P value < 2.2e-16) (Fig. 4b).
301 Our data suggests that the dynamic increase in the number of enhancer OEs connected
302 to a promoter results in an overall increase in expression of genes, in agreement with
303 the current models of transcriptional control *via* enhancer-promoter interactions[37,38].
304

305 To further explore the specific role of rewired promoter-anchored interactions in the
306 altered transcriptional program, we evaluated which transcription factors (TFs) are
307 associated with these gained interactions. Notably key transcription factors involved in
308 ER+ breast cancer were highly enriched, including methylation-sensitive ER (estrogen
309 response elements (EREs)) and ELF5 (ETS transcription factor family members), as
310 well as architectural proteins CTCF and ZNF165 (Fig. 4c).
311
312 Because of the known role of ER transcription factor in inducing 3D chromatin
313 interactions in ER+ breast cancer cells[14,39-41] and methylation-sensitive binding[42], we
314 profiled ER binding site (ERBS) patterns genome-wide in Vehicle (n = 4) and
315 Decitabine-treated (n = 4) tumours via ER ChIP-seq to determine if ER binding was
316 specifically altered by DNA hypomethylation. Differential binding analyses (Diffbind[6])
317 revealed reprogramming of the ER binding characterised by 1095 gained ERBS and
318 279 lost ERBS following Decitabine treatment as compared to Vehicle (FDR < 5%)
319 (Fig. 4d) and a stronger average ER ChIP-seq signal at gained ERBS in Decitabine
320 samples as compared to Vehicle, while lost sites showed a moderate decrease in binding
321 intensity genome-wide (Fig. 4e).
322
323 Remarkably, over 75% of all gained ERBS were located at distal regulatory regions
324 associated with active and poised enhancers (Fig. 4f and Extended Data Fig. 4b), and
325 these sites were enriched for the estrogen response elements (EREs) DNA motif,
326 followed by FOXA1 (Fig. 4g). Lost ERBS were most frequently positioned close to a
327 TSS (> 40% less than 1Kb from TSS) (Extended Data Fig. 4b), were associated with
328 active promoters (Extended Data Fig. 4c) and were enriched for Sp1 and NFY promoter
329 DNA motifs (Extended Data Fig. 4d). Both lost and gained ERBS were highly enriched
330 for the FOXA1 motif (Fig. 4g and Extended Data Fig. 4d). Additionally, we found a
331 significant loss (approx. 44.4%) of DNA methylation at gained ERBS (Fig. 4h and
332 Extended Data Fig. 4f), as illustrated in Figure 4i at the *ANKRD2* gene locus (Fig. 4i,
333 further example in Extended Data Fig. 4g). In contrast the small proportion of ERBS
334 that were lost remained unmethylated in both Vehicle and Decitabine treated samples
335 (approx. 6.92% DNA methylation change; Extended Data Fig. 4h), suggesting that this
336 subset of ERBS were altered independently of a direct change in DNA methylation.
337

338 **Rewired ER-bound chromatin interactions are associated with activation of ER**
339 **target genes**
340 To determine whether this gain in ER-enhancer binding was associated with rewired
341 3D chromatin interactions, we integrated the gained ERBS with ectopic enhancer-
342 promoter interactions and associated transcriptional programs. Consistent with ERE
343 motifs enriched at gained enhancer OEs (Fig. 4c), we found significant enrichment for
344 gained ER binding sites (Fig. 5a) and a genome-wide increase in ER binding density at
345 ectopic enhancer OEs induced by Decitabine treatment (Fig. 5b). We propose that these
346 ER-associated enhancer-promoter interactions are mediated by a change in ER binding
347 at enhancer OEs ("ER-bound interactions").
348
349 We next specifically focused on these gained ER-bound enhancer-promoter
350 interactions in detail by identifying connected genes and comparing their expression
351 between Vehicle and Decitabine tumours. The majority (~74%) of these genes
352 showed an overall increase in expression following Decitabine treatment (Fig. 5c) and
353 included established ER target genes (for example *B4GALT1, MYO3B, SEMA3G*) as
354 well as genes associated with a good clinical outcome in ER+ breast cancer (for
355 example *SPATA18, SCUBE2, GALNT5, IGFBP4*). For example, at the *SPATA18*
356 locus, multiple 3D enhancer-promoter interactions are gained with Decitabine
357 treatment, concomitant with gain in ER binding at putative enhancer, loss of DNA
358 methylation and activation of the ER target gene (Fig. 5d and Extended Data Fig. 5a).
359 Moreover, high expression of *SPATA18* gene is associated with good prognosis in
360 ER+ breast cancer (Extended Data Fig. 5a). *SCUBE2* (Fig. 5e and Extended Data Fig.
361 5b), *B4GALT1* (Fig. 5f and Extended Data Fig. 5c) and *MYO3B* (Extended Data Fig.
362 5d) genes also exemplify the relationship between Decitabine-induced gain of
363 multiple ER-bound enhancer-promoter interactions and activation of their ER target
364 genes that are associated with good prognosis in ER+ breast cancer.
365
366 Taken together, these results reveal a link between Decitabine-induced DNA
367 hypomethylation, rewiring of ER-bound enhancer-promoter interactions and alteration
368 in the ER transcriptional program.
369
370 **Dynamics of DNA hypomethylation and re-methylation on 3D chromatin**
371 **interactions**

372 Finally, to determine the dynamics between DNA methylation alterations and 3D
373 enhancer -promoter rewiring and expression changes, we performed a time-course of
374 Decitabine followed by period of long term recovery in an established cell line model
375 of endocrine-resistance TAMR[14,43,44] cells. Low dose Decitabine was applied daily for
376 7 days to induce hypomethylation, followed by a recovery time-point (28 days) to
377 allow for re-methylation of CpG sites demethylated by Decitabine (Fig. 6a). We
378 confirmed loss and recovery of DNMT1 protein expression by Western blot (see
379 Supplementary Note). We assessed changes in DNA methylation, RNA expression
380 and 3D enhancer-promoter interactions on day 7 Decitabine- ("Day 7 Decitabine")
381 and day 28 post-Decitabine ("Decitabine Recovery"), as well as passage-matched
382 control cells ("Early Control" and "Late Control") in duplicate. As expected, 7 day
383 Decitabine treatment resulted in widespread DNA hypomethylation in the TAMR
384 cells (approx. 41.84% change in median DNA methylation, *P* value < 0.0001, two-
385 tailed Mann-Whitney test; Fig. 6b and Extended Data Fig. 6a). Substantial genome-
386 wide recovery of DNA methylation was also observed following 28 days of recovery
387 compared to matched vehicle-treated control (approx. 25.46% change in median DNA
388 methylation, *P* value < 0.0001, two-tailed Mann-Whitney test; Fig. 6b and Extended
389 Data Fig. 6a). Similar to the PDX Decitabine-treated samples, we found that DNA
390 hypomethylation changes in TAMR cells, after 7 days of Decitabine treatment, were
391 enriched for ChromHMM [14] enhancers (Fig. 6c) and ER binding sites[6] (Fig. 6d).
392
393 To study the dynamics of DNA re-methylation on 3D chromatin interactions, we first
394 identified DNA regions that were substantially re-methylated after 28 days of
395 recovery in "Decitabine Recovery" samples, as compared to "Day 7 Decitabine"
396 samples (>30% gain in DNA methylation; Supplementary Table 1). We found that the
397 regions that re-gained DNA methylation were also enriched in poised enhancers and
398 depleted at promoter regions (Fig. 6e). In fact, 10,195 probes located at ChromHMM
399 enhancers hypomethylated after day 7 Decitabine treatment, gained methylation after
400 28-days recovery (Extended Data Fig. 6b) and were also enriched for ER binding[6]
401 (Fig. 6d). To determine if 3D enhancer-promoter interactions were also altered in the
402 Decitabine time course, we performed Promoter Capture Hi-C. We found that
403 chromatin interactions separate the control and Decitabine-treated samples on X-axis,
404 with Decitabine Recovery samples clustering together with control samples and away
405 from the Day 7 Decitabine samples on the Y-axis, suggesting substantial "recovery"

406 of chromatin interactions 28 days post Decitabine treatment (Extended Data Fig. 6c).
407 Similar to the PDX results (Fig. 3f), we found that Day 7 Decitabine-treated TAMR
408 samples resulted in a large gain in the number of new enhancer OEs connected to bait
409 promoters (Fig. 6f). Moreover, these additional ectopic interactions were mostly lost
410 in Decitabine Recovery (Fig. 6g). Importantly, the majority of Day 7 Decitabine
411 gained OE enhancers (64,044) interactions were lost in Decitabine Recovery samples
412 (47,007 OE enhancers "recovered" interactions) (Fig. 6h).
413
414 We found that gained enhancer-promoter interactions at Day 7 Decitabine treatment,
415 were significantly associated with an overall increase in gene expression (195 up-
416 regulated genes (P value < 0.05; logFC > 1.5; Fisher's exact test P value < 2.2e-16)
417 (Fig. 7a). No significant increase in expression for genes at Decitabine Recovery
418 interactions was observed (49 up-regulated genes; Fisher's exact test P value =
419 0.3167) (Fig. 7b). After 28 days of "recovery" we observed that loss of gene
420 expression was concordant with reversal of ectopic enhancer-promoter interactions,
421 including at key ER-target genes (Fig. 7b). Further evidence of a direct relationship
422 between DNA hypomethylation and ectopic 3D enhancer-promoter interactions is
423 exemplified at ER-target genes also identified in the PDX data: *SPATA18* (Fig. 7c),
424 *B4GALT* (Fig. 7d), *EVL* and *MYO3B* (Extended Data Fig. 6d-e). Notably, we also
425 found a subset of genes that remained upregulated after 28 days of "recovery", for
426 example *SCUBE2,* where the chromatin contacts were still not fully resolved
427 (Extended Data Fig. 6f).
428
429 **Discussion**
430 Three-dimensional (3D) epigenome remodelling, including widespread changes to
431 DNA methylation and 3D chromatin structure, is an emerging mechanism of gene
432 deregulation in cancer. Our previous work demonstrated that DNA hypermethylation
433 and concomitant loss of ER binding at enhancers was a key event associated with
434 alterations in 3D chromatin interactions in ER+ endocrine-resistant breast cancer[45].
435 Therefore, we were motivated to determine if these 3D chromatin alterations could be
436 resolved with epigenetic therapies that induce DNA hypomethylation. To date, most
437 studies investigating the use of epigenetic therapies have focused on assessing efficacy
438 in blood cancers and activation of the immune system *via* viral mimicry response.
439 While some studies demonstrated that Decitabine treatment has anti-tumour properties

440 in solid cancers (reviewed in [46]), the exact mechanism that underpins this response was
441 unclear and evidence for therapeutic activity was inconclusive[21,46].
442
443 Here, using patient-derived xenograft models of ER+ endocrine-resistant breast cancer,
444 we show that treatment with Decitabine induced DNA hypomethylation and had potent
445 anti-tumour activity associated with suppression of tumour growth and cell
446 proliferation gene pathways. To assess the broader functional impact of DNA
447 hypomethylation, we analysed multiple layers of 3D genome organisation, including
448 chromosomal compartments, TADs and 3D chromatin interactions and integrated the
449 3D data with DNA methylation, transcriptome and ER transcription factor profiles in
450 Decitabine and Vehicle-treated PDX tumours. Collectively our data supports a model
451 (Fig. 8), whereby low dose Decitabine treatment results in enhancer DNA
452 hypomethylation, reprogramming of ER chromatin binding, and rewiring of enhancer-
453 promoter interactions, leading to activation of ER target genes. Importantly, we
454 identified rewired ER-bound chromatin interactions that connect ER-enhancers to
455 specific target genes, which included Estrogen Response Hallmark genes involved in
456 cell cycle inhibition and tumor suppression. Finally, we confirm a mechanistic link
457 between Decitabine-induced DNA hypomethylation, rewiring of 3D chromatin
458 interactions and gene activation using "rescue" DNA methylation experiments in a cell
459 line model of endocrine-resistant breast cancer.
460
461 Decitabine has been previously demonstrated to have some therapeutic efficacy in
462 multiple subtypes of breast cancer and in overcoming drug resistance[4,47]. Transient low-
463 dose treatment with Decitabine resulted in decrease in promoter DNA methylation,
464 gene re-expression, and had antitumor effect *in vivo* in breast cancer cells[48]. Low-dose
465 Decitabine has also been shown to prevent cancer recurrence by disrupting the pre-
466 metastatic environment through its effect on myeloid-derived suppressor cells in breast
467 and other cancers[49]. In triple negative breast cancer (TNBC) PDX organoids,
468 Decitabine sensitivity was positively correlated with protein levels of DNMTs,
469 suggesting DNMT levels as potential biomarkers of response[50]. A recent study of
470 Decitabine in a panel of breast cancer cell lines observed that Decitabine also induced
471 genes within apoptosis, cell cycle, stress, and immune pathways[51]. However,
472 knockdown of key effectors of the immune pathway did not affect Decitabine

473 sensitivity suggesting that breast cancer growth suppression by Decitabine is
474 independent of viral mimicry[51].
475
476 We found that the low dose Decitabine treatment resulted in minimal DNA
477 hypomethylation at repetitive elements. Despite this, we observed a relatively large
478 number of TEs becoming activated with treatment, consistent with previous studies in
479 cancer cell lines[52]. Loss of DNA methylation at repetitive elements and expression of
480 TEs has been shown to drive viral mimicry response in tumours treated with epigenetic
481 therapies[24-26]. In agreement with studies in colorectal tumour cells[24,53], our results
482 indicate that treatment with Decitabine results in up-regulation of multiple immune
483 pathways (Interferon and Inflammatory Response pathways), which could promote
484 anti-tumour immunity. However, immunodeficient NOD-*scid IL2rγ*^{null} (NSG) mice
485 required for PDX experiments in our study largely lack mature immune cells and
486 therefore the potential immune response could not solely account for the tumour
487 inhibitory effects of Decitabine treatment observed in our study. This highlights the
488 need to study both the immune-based and tumour-based mechanisms that underpin
489 response to epigenetic therapies.
490
491 There have been limited studies to date on the role of DNA methylation in shaping the
492 3D genome organisation[14,16,54-56]. Simultaneous profiling of DNA methylation and 3D
493 genome in single cells revealed pervasive interactions between these two epigenetic
494 layers in regulating gene expression[57]. Additionally, binding of CCCTC-binding factor
495 (CTCF), an insulator protein involved in creating chromatin loops and domain
496 boundaries has been shown to be methylation-sensitive[58-61]. DNA hypermethylation at
497 CTCF binding site in *IDH* mutant gliomas results in its reduced CTCF binding, loss of
498 insulation between topological domains and aberrant gene activation[16]. More recently,
499 DNA hypomethylation has been shown to result in de-compaction of chromatin and
500 loss of compartmental organisation[53,56,62,63]. This is consistent with our data showing
501 closed (B-type) to active (A-type) compartment shifting with Decitabine-induced DNA
502 hypomethylation and reduced interactions between B-type compartments.
503
504 A number of studies have suggested an important role of DNA methylation in altering
505 ER binding at regulatory elements[44,64], however no studies have examined the potential
506 effect on ER-bound 3D chromatin interaction. We have previously shown that DNA

507 methylation differences at enhancers underpin differential ER binding events
508 associated with endocrine resistance[44]. Furthermore, recent studies demonstrated that
509 ER-bound 3D chromatin interactions are altered in endocrine-resistant cells[14,15]. In this
510 study, we show that Decitabine-induced DNA hypomethylation at ER-bound enhancers
511 plays an important functional role in promoting ectopic 3D chromatin interactions and
512 we identify key ER-bound chromatin interactions that control expression of genes
513 associated with endocrine-resistant tumour growth suppression. These results add to
514 the current research, showing that enhancer reprogramming through transcription factor
515 binding or chromatin remodelling can promote transcriptional programs that are
516 associated with endocrine response in breast cancer[65,66].
517
518 Our high-resolution promoter interactions data also revealed an increase in the number
519 of interacting enhancers connecting to gene promoters induced by Decitabine. We
520 hypothesise that the overall increase in enhancer connectivity results in creation of
521 active transcription hubs[38] or frequently interacting regions[67] at activated genes, which
522 will be investigated in future studies. This is in agreement with recent reports of
523 transcriptional activation occurring in non-membrane bound nuclear compartments that
524 harbour multiway enhancer-promoter interacting hubs[68] as well as additive effect of
525 multiway enhancer interactions on gene expression[69].
526
527 In summary, our work highlights a novel molecular mechanism of epigenetic therapies
528 in endocrine-resistant ER+ breast cancer. We provide mechanistic insights into how
529 Decitabine-induced DNA hypomethylation promotes 3D epigenome remodelling
530 including rewiring of ER-mediated 3D enhancer-promoter chromatin interactions.
531 Epigenetic therapy therefore has the potential to overcome cancer therapy resistance by
532 targeting the 3D epigenome architecture to resolve gene deregulation and reduce cancer
533 growth.

534 **Methods**

535

536 **Patient-derived xenograft (PDX) models of ER+ breast cancer**

537 All *in vivo* experiments, procedures and endpoints were approved by the Garvan
538 Institute of Medical Research Animal Ethics Committee (HREC #14/35, #15/25) and
539 performed at the Garvan Institute of Medical Research using standard techniques as
540 described previously [27,70] in accordance with relevant national and international
541 guidelines. The Gar15-13 model was generated in-house at the St Vincent's Hospital
542 under the Human Research Ethics protocol (HREC/16/SVH/29) and the HCI-005
543 model was developed by the Welm laboratory at the Huntsman Cancer Institute
544 (University of Utah)[70]. Gar15-13 was derived from a resected breast cancer liver
545 metastasis of ER-positive, PR-negative, HER2-negative metastatic breast cancer[28].
546 HCI-005 was derived from a pleural effusion of ER-positive (ERmutL536P), PR-
547 positive, HER2-positive metastatic breast cancer. Growth of HCI-005 was supported
548 by estrogen supplementation in the form of a 60 day 17-β-estradiol pellet implanted
549 simultaneously with the tumour chunks. Mice implanted with Gar15-13 did not receive
550 estrogen supplementation as this model does not require additional estrogen for
551 growth[28].

552

553 At surgery, 4 mm^3 sections of tumour tissue were implanted into the 4th inguinal
554 mammary gland of 6–8-week-old female NOD-*scid* IL2Rγ^{null} (NSG) mice, obtained
555 from Australian BioResources (Sydney, Australia). For HCI-005, tumour growth was
556 supported by implantation of an E2 pellet inserted subcutaneously via the incision site
557 before it was sealed with an Autoclip wound clip. When tumours became palpable,
558 tumour growth was assessed twice weekly by calliper measurement (using the formula:
559 $width^2 \times length/2$) and mice were randomised to treatment arms when tumours reached
560 200 mm^3 using an online randomisation tool
561 (https://www.graphpad.com/quickcalcs/randomize1.cfm) (n = 6 - 8 mice per group for
562 therapeutic studies, exact numbers specified in figure legends).

563

564 **Pharmacological treatments in PDX models**

565 The DNA methyltransferase inhibitor, Decitabine (5-Aza-2'-deoxycytidine: Sigma, Cat
566 #3656) was reconstituted in PBS and stored at -80°C.

567 Decitabine was administrated in 0.5mg/kg/mouse dose in PBS 100ul IP 2 times weekly.
568 Vehicle mice were treated with 100µl PBS IP. Mice were treated for 60 days or until
569 tumour volume reached 1000 mm^3. Upon reaching ethical or pre-defined experimental
570 endpoints, mice were euthanized, and the primary tumour collected. After weighing,
571 the tumour was cut into pieces that were allocated to be snap-frozen, fixed overnight at
572 4°C in 10% neutral-buffered formalin, or embedded in cryo-protective optimal cutting
573 temperature (OCT) compound before being snap frozen. Frozen samples were kept at
574 -80°C. Formalin-fixed samples were sent to the Garvan Institute Histology Core
575 Facility for paraffin embedding. Tumour growth curves were analysed in GraphPad
576 Prism (GraphPad Software) by two-tailed, unpaired t-test. Tumour mass at end-point
577 was analysed by two-tailed Mann-Whitney t-test as per figure legends unless otherwise
578 specified.
579
580 **Cell culture**
581 MCF7 breast cancer cells and the corresponding endocrine-resistant sub-cell lines were
582 kindly given to our laboratory by Dr. Julia Gee (Cardiff University, UK). Tamoxifen-
583 resistant MCF7 cells (TAMR) were previously generated by the long-term culture of
584 MCF7 cells in phenol red-free RPMI medium containing 10% charcoal-stripped FBS
585 (Gibco) and 4-OH-tamoxifen (1×10^{-7} M; TAM).
586
587 **Pharmacological treatments in cell lines**
588 Cells were treated daily with Decitabine (100nM) for 7 consecutive days. After 7
589 days, fresh media was added, and cells were harvested at day 7 ("Decitabine Day 7").
590 Control cells were cultured for a total of 11 days in normal media and harvested for
591 "Control Early" on day 11. For the "Decitabine Recovery" samples, cells were treated
592 daily with Decitabine (100nM) for 7 consecutive days, after which fresh media was
593 added; cells were cultured for 21 additional days and harvested on day 28 ("recovery"
594 - reintroduction of DNA methylation). Matched control cells were cultured for 28
595 days in normal media and harvested at day 28 for "Control Late". DNMT1 protein
596 levels were confirmed by Western blot (see Supplementary Note).
597
598 **Cellular viability assay**
599 Tamoxifen-resistant (TAMR) MCF7 cells were seeded in a white flat-bottom 96-well
600 plate at a density of 2500 cells/well based on doubling time and allowed to adhere

601 overnight. Cells were treated daily with Decitabine (0nM, 10nM, 50nM, 100nM,
602 200nM, 300nM, 500nM, 1uM, 5uM, 10uM and 100uM) for 72h and cellular viability
603 was assessed on day 5, following 2 days of recovery using the alamarBlue
604 (ThermoFisher, DAL1025) assay in accordance with the manufacture's
605 recommendations (see Supplementary Note).
606
607 **Immunohistochemistry (IHC) and quantification**
608 Tumour tissue was harvested and immediately fixed in 10% neutral buffered formalin
609 at 4°C overnight before dehydration and paraffin embedding. Antibodies used for IHC
610 were anti-ER (M7047, 1:300, Agilent) and anti-Ki67 (M7240, 1:400, Agilent). Primary
611 antibodies were detected using biotinylated IgG secondary antibodies (Agilent, 1:400),
612 using streptavidin-HRP (Agilent) for amplification of signal followed by the addition
613 of 3,3′-diaminobenzidine (Sigma) substrate. Images were scanned using Leica Aperio
614 Slide Scanner (Leica Biosystems) and analysed using QuPath software to differentiate
615 tumour tissue from stroma and necrosis, and to quantify Ki-67 positivity in tumour
616 tissue.
617
618 **Low input *in situ* Hi-C in snap-frozen PDX tumour samples and TAMR cells**
619 Tumour tissue samples were flash frozen and pulverized in liquid nitrogen before
620 formaldehyde cross-linking in TC buffer. Hi-C was then conducted using the Arima-
621 HiC kit, according to the manufacturer's protocols (Cat. #A510008) with minor
622 modifications. Briefly, for each Hi-C reaction between ~100,000 - 500,000 cells were
623 cross-linked with 2% formaldehyde and nuclei were isolated by incubating cross-linked
624 cells in Lysis Buffer at 4°C for 30 minutes. The Arima kit uses two restriction enzymes
625 recognizing the following sequence motifs ^GATC and G^ANTC (N can be either of
626 the 4 genomic bases), which after ligation of DNA ends generates 4 possible ligation
627 junctions in the chimeric reads: GATC-GATC, GANT-GATC, GANT-ANTC, GATC-
628 ANTC. Hi-C libraries were prepared using the Swift Biosciences Accel-NGS 2S Plus
629 DNA Library Kit with a modified protocol provided by Arima with 8 PCR cycles for
630 library amplification as required. Hi-C libraries were sequenced on Illumina HiSeq X10
631 in 150bp paired-end mode.
632
633 **Promoter Capture Hi-C**

634 To perform promoter Capture Hi-C (PCHi-C), we computationally designed RNA
635 probes that capture promoter regions of previously annotated human protein-coding
636 genes. Promoter Capture was performed as previously described[71-73] using the Arima
637 HiC+ kit for Promoter CHi-C (human) (Cat #A510008, #A303010, #A302010 and
638 #A301010). First, to identify promoter capture targets, 23,711 unique Ensembl
639 annotated genes were extracted from the GRCh38 gene annotation file in Ensembl
640 database, version 95. These compromised of protein-coding (18,741), antisense (84),
641 lincRNA (170), miRNA (1,878), snoRNA (938), snRNA (1,898) or multiple (2)
642 transcripts. We then located transcription start sites (TSS) of each gene and mapped the
643 TSS coordinates to the in silico digested genome (^GATC and G^ANTC) and extracted
644 the restriction fragment containing the TSS, as well as one restriction fragment
645 upstream and one restriction fragment downstream for each TSS. The final target list
646 of TSS mapped to 3 consecutive restriction fragments. The average length of the 3
647 consecutive restriction fragments for each TSS is 786bp and the median is 927bp, with
648 a range of 54-4174bp.
649 Moreover, for the individual restriction fragments smaller than 700bp, all nucleotides
650 within these fragments are less than or equal to 350bp from the nearest cut site, and
651 therefore the entire restriction fragment was defined as a target region for subsequent
652 probe design. This scenario represents the vast majority of cases, because the mean
653 length of an individual restriction fragment is 263bp, with a median of 431bp. However,
654 if an individual restriction fragment was greater than 700bp, then the 350bp on each
655 inward facing edge of the restriction fragment was defined as a target region for probe
656 design, and the centre most portion of the restriction fragment was excluded from the
657 probe design. After this final processing, a final BED file of target bait regions was
658 input into the Agilent SureDesign tool, and probes were designed using a 1X tiling
659 approach, with moderate repeat masking and balanced boosting. Promoter Capture was
660 carried out using Hi-C libraries from three Vehicle-treated tumour samples and three
661 Decitabine-treated tumour samples with the SureSelect target enrichment system and
662 RNA bait library according to manufacturer's instructions (Agilent Technologies kit),
663 using 12 post-capture PCR cycles as required. PCHi-C libraries were sequenced on the
664 Illumina HiSeq X10 platform in 150bp paired-end mode.
665
666 **Microarray genome-wide DNA methylation**

667 DNA from four Decitabine and four Vehicle-treated tumours from two PDX models
668 (Gar15-13 and HCI-005) was isolated from snap-frozen tumour samples using the
669 Qiagen QIAamp DNA Mini Kit. DNA (500ng) was treated with sodium bisulphite
670 using EZ-96 DNA methylation kit (Zymo Research CA, USA). DNA methylation was
671 quantified using the Illumina InfiniumMethylationEPIC (EPIC) BeadChip (Illumina,
672 CA, USA) run on the HiScan System (Illumina, CA, USA) using manufacturer's
673 standard protocol.
674
675 **ChIP-seq**
676 Tumour samples were snap-frozen in Optimal Cutting Temperature compound (Tissue-
677 Tek) and used for ER ChIP-seq experiments. Using a cryostat (Leica, #CM3050-S), a
678 minimum of 50 x 30 µm sections were cut from each tumour at -20℃ and subjected to
679 double cross-linking with DSG and formaldehyde as previously described[30]. ER ChIP-
680 seq was performed with an anti-ER antibody (Santa Cruz, SC-543X). 5µg of antibody
681 was used to ChIP each tumour sample and 10ng of immunoprecipitated DNA was
682 submitted to the David R. Gunn Genomics Facility at the South Australian Health and
683 Medical Research Institute (SAHMRI) for sequencing. Conversion of the DNA into
684 sequencing libraries was performed using the Ultralow Input Library Kit (Qiagen,
685 #180495) and sequenced on the Illumina NextSeq 500 (Illumina) in 75bp single-end
686 mode to achieve a minimum of 20 million reads per sample.
687
688 **RNA-seq**
689 RNA was extracted from snap-frozen tumour PDX tissue and TAMR cell line samples
690 using the RNeasy Mini Kit (QIAGEN) and quality of purified RNA was confirmed
691 with RNA ScreenTape TapeStation (Agilent). All samples processed for RNA-seq had
692 a RIN equivalent (RIN^e) quality score ≥ 8.0. Total RNA was supplied to the genomics
693 core facility (Kinghorn Centre for Clinical Genomics) for library preparation and
694 sequencing. RNA was prepared for sequencing using the TruSeq Stranded mRNA
695 Library Prep kit (Illumina) and libraries were sequenced on Illumina NovaSeq 6000 S4
696 in paired-end mode.
697
698 **EPIC DNA methylation analyses**
699 Raw intensity data (IDAT) files were imported and quality controlled using *minfi*
700 package (v.1.34.0)[74]. Data was then normalised with background correction. To reduce

701 the risk of false discoveries, we removed probes affected for cross-hybridization to
702 multiple locations on the genome or overlapped SNPs, as previously described[75]. Beta
703 (β) values were calculated from unmethylated (U) and methylated (M) signal [M/(U +
704 M + 100)] and ranged from 0 to 1 (0 to 100% methylation). β values of loci whose
705 detection P values were > 0.01 were assigned NA in the output file. To map EPIC arrays
706 to hg38/GRCh38 assembly, all probes were annotated with the
707 EPIC.hg38.manifest.tsv.gz files as described in[76].
708 For initial visualisation of the EPIC data, multidimensional scaling plots were generated
709 using the 'mdsPlot' function in the *minfi* Bioconductor package (v.1.34.0)[74].
710 Differential analyses were then performed between treatment arm with Decitabine
711 versus Vehicle samples. For each comparison, β values were transformed using logit
712 transformation: $M = \log2(\beta/(1-\beta))$. We used the limma package (v.3.46)[77] to identify
713 DMPs between sample groups with adjusted *P* value cut-off of < 0.01. The R package
714 DMRcate (v.2.2.3)[78] was used to identify DMRs, with DMP *P* value cut-offs of FDR <
715 0.01. DMRs were defined as regions with a maximum of 1000 nucleotides between
716 consecutive probes and a minimum of 2 CpG sites, a methylation change > 30% and
717 we applied Benjamini-Hochberg correction for multiple testing. ChromHMM data
718 downloaded from GEO (GSE73783) for tamoxifen-resistant (TAMR) MCF7 cells was
719 used to annotate DMPs to chromatin states. REMP R package (v.1.14.0)[32] was used to
720 assess genome-wide locus-specific DNA methylation of repeat elements (LTR, LINE1
721 and Alu) from EPIC data with IlluminaHumanMethylationEPICanno.ilm10b5.hg38
722 annotation (GitHub).
723
724 **Hi-C analyses**
725 Hi-C sequenced reads (150bp paired-end) were quality checked with FastQ Screen
726 v.0.14.1[79] for mouse host reads contamination. Reads were then processed with
727 Xenome (v.1.0.1)[80] as described in [81]. Remaining reads were aligned to the human
728 genome (hg38/GRCh38) using HiC-Pro[82] (v.2.11.4). Initially, to generate Hi-C contact
729 matrices, the aligned Hi-C reads were filtered and corrected using the ICE "correction"
730 algorithm[83] built into HiC-Pro, which corrects for the CNV-related variability in the
731 tumours[84]. Inter-chromosomal interactions were excluded from further analyses to
732 control for the effect of inter-chromosomal translocations in the tumours. Contact
733 matrices for 3D genome feature annotation and visualisation were created and Knight-
734 Ruiz (KR) normalized using Juicer tools[85] using contact matrices in .hic format

735 generated by hicpro2juciebox script in HiC-Pro as input (hic file version 8). Hi-C
736 matrices were visualised using JuiceBox[86] and WashU Epigenome Browser[87]. We
737 confirmed data quality by assessing the proportion of cis/trans interactions and
738 percentage of valid fragments for each library. Overall, we obtained an average of 100
739 million unique, valid contacts per replicate (~310 million per treatment arm), for an
740 average resolution of 10kb. Statistics for each library can be found in Supplemental
741 Table 2. These data was used to derive loops, TAD boundaries and chromosomal
742 compartment structures.
743
744 **Insulation score and identification of TAD boundaries**
745 Topological domain boundary calling was performed by calculating insulation scores
746 in ICE normalised contact matrices at 20kb resolution using TADtool[88]. To identify
747 appropriate parameters, we called TADs across chromosome 1 using contact matrices
748 at 20kb and threshold values: 10, 50 and 100. The final TADs were called for all
749 chromosomes at window 102353 and cut-off value 50. Boundaries that were found
750 overlapping by at least 1 genomic bin were merged. Boundaries separated by at least
751 one genomic bin were considered different between datasets. Pyramid-like heatmap
752 plots were generated with GENOVA[89].
753
754 **Identification of compartments A and B**
755 For each chromosome in each sample, compartments where called using the standard
756 PCA method[33] in Homer package (version 4.8). The resolution was set to 50kb and the
757 window size to 100 kb. Compartments were defined as regions of continuous positive
758 or negative PC1 values using the findHiCCompartments.pl tool in Homer. To detect
759 which compartment is the open "A-type" and which is the closed "B-type," the genome-
760 wide gene density was calculated to assign the "A-type" and "B-type"
761 compartmentalisation. To identify genomic regions that switch between two
762 compartment types, we used correlation difference script (getHiCcorrDiff.pl) with
763 findHiCCompartments.pl tool in Homer. Compartments were considered common if
764 they had the same compartment definition within the same genomic bin. Compartment
765 changes between treatment arms were computed after considering compartments that
766 were overlapping between biological replicates, unless otherwise indicated.
767 To directly quantify the tendency of each region to interact with the other regions in
768 either A or B compartments, we calculated the "A/B interaction ratio", defined for each

769 100kb genomic window as the ratio of interaction frequency with A versus B
770 compartments using O/E matrix with GENOVA[89] (v1.0.0,
771 https://github.com/robinweide/GENOVA). Log_2 contact enrichments were plotted as a
772 heat saddle plot. Summarised A-A, B-B and B-A compartment strengths were
773 calculated as the mean log_2 contact enrichment between the top (A) or bottom (B) 20%
774 of PC1 percentiles. The compartment strength ratio was calculated as log_2(A-A/B-B).
775
776 **PCHi-C analyses**
777 PCHi-C sequenced reads were mapped and filtered using HiCUP (v.0.7.4)[90] with
778 hg38/GRCh38 genome digested with –arima flag and minimum di-tag length set to 20.
779 Statistics for each library can be found in Supplementary Table 3. On target rate was
780 calculated by counting number of valid, unique reads overlapping bait fragments (min.
781 overlap > 0.6). Unique, valid mapped reads from HiCUP were converted into .chinput
782 files using bam2chicago.sh utility and obtained chinput files were further filtered and
783 processed with CHiCAGO (v.1.14.0)[34]. CHiCAGO design files were created with
784 following parameters to account for multiple restriction enzymes used in the Arima
785 HiC kit and the Arima-specific design of the bait fragments: MaxLBrowndist = 75000;
786 binsize = 1500; minFragLen = 25; maxFragLen = 1200. Significant interactions were
787 called with CHiCAGO using score cut-off of 5. All bait-to-bait interactions were
788 discarded. Chicdiff package[35] (v.0.6) was used to compare PCHi-C data from Vehicle
789 and Decitabine tumours and the difference in the mean asinh-transformed CHiCAGO
790 scores between conditions above 1 was used to prioritise the potential differential
791 promoter-anchored interactions. Only interactions that have CHiCAGO score of more
792 than 5 in at least 2 replicates were included for downstream analysis. Volcano plots
793 were generated using EnhancedVolcano R package (v.1.8.0)[91]. For downstream
794 analysis of merged replicate data and for visualisation of interactions in WashU
795 Epigenome Browser[87] replicates were merged with CHiCAGO. We defined
796 reprogrammed enhancer-promoter interactions by constructing a consensus, gained and
797 lost subset of promoter-anchors (baits) and other end anchors (OEs) based on
798 CHiCAGO promoter interactions, Chicdiff analysis and setdiff R function across the
799 replicates. The following criteria was used to obtain these regions: CHiCAGO score >
800 5 in 2 out of 3 replicates in either condition, Chicdiff generated asinh-transformed
801 CHiCAGO scores between conditions above 1 and no overlap between regions,
802 allowing for 10Kb maximal gap in 3 out of 3 replicates. ChromHMM data downloaded

803 from GEO (GSE73783) for tamoxifen-resistant (TAMR) MCF7 cells was used to
804 annotate promoter-anchored interactions to chromatin states.
805
806 **RNA-seq data analyses**
807 For canonical gene expression, RNA-seq raw reads were quality checked (FastQ Screen
808 v.0.14.1[79]). Sequence adaptors were trimmed using Trim Galore (v.0.11.2), reads were
809 processed with Xenome v.10.1.[80] to remove mouse sequences and remaining reads were
810 mapped with STAR (v.2.7.7a)[92] to the hg38/GRCh38 human genome build with
811 GENCODE v33 used as a reference transcriptome (parameter settings: –quantMode
812 TranscriptomeSAM–outFilterMatchNmin 101 –outFilterMultimapNmax 20). Statistics
813 for each library can be found in Supplementary Table 4. TMM normalisation was
814 applied to normalise for RNA composition[93] and differential expression was performed
815 with edgeR 3.18.1 [94] using the generalised linear model (GLM). RNA-seq tracks were
816 generated using bedtools v.2.22 genomeCoverageBed to create normalised.bedGraph
817 files and bedGraphToBigWig (USCS utils) to create.bigwig files.
818 For analysis of TE expression, adapter-trimmed, human-only RNA-seq reads were
819 mapped with STAR (v.2.7.7a), allowing for multimapping alignments (flags: --
820 outFilterMultimapNmax 100 --outFilterMismatchNmax 100). Annotation GTF files for
821 canonical genes were downloaded from Ensembl genome browser (v.102,
822 GRCh38.p13 assembly) and TE annotation GTF file
823 (GRCm38_Ensembl_rmsk_TE.gtf) was downloaded from TEtranscripts [95] website
824 (http://hammelllab.labsites.cshl.edu/software/#TEtranscripts). Normalisation and
825 differential expression was performed for all genes and TEs using DESeq2[96]. TEs with
826 and FDR < 0.1 and logFC > 0.7 were considered differentially expressed in pair-wise
827 comparisons. Volcano plots were generated using EnhancedVolcano R package
828 (v.1.8.0)[91].
829
830 **ChIP-seq data analyses**
831 ChIP-seq reads were aligned against human genome (hg38/GRCh38) using bowtie2
832 with default parameters[97]. Non-uniquely mapped, low quality (MAPQ < 15) and PCR
833 duplicate reads were removed. Peak calling of individual ChIP–seq experiments was
834 performed with MACS2 with default parameters[98,99]. Statistics for each library can be
835 found in Supplementary Table 5. Consensus peaks were identified by intersecting
836 MACS2 peaks obtained from each sample using bedtools intersect (v.2.25.0) with min.

837 overlap > 0.6. Differential binding analyses were performed using DiffBind (v.3.0.9)[6]
838 and DESeq2 (v.1.3.0)[96] with FDR < 5%. Enrichment analyses were performed using
839 GAT[100], ChIPseeker (v.1.26.0)[101] and normalised to library size. Merged bigwig tracks
840 for visualisation were created from merged bam files from all replicates using the
841 bamCoverage function with scaling factor normalisation and heatmaps and average
842 profiles were plotted with deepTools2[102]. ChromHMM data downloaded from GEO
843 (GSE73783) for tamoxifen-resistant (TAMR) MCF7 cells was used to annotate ER
844 binding sites to chromatin states. The Homer motif discovery suite[103] was used for motif
845 analysis using the bed regions from differential peaks detected by DiffBind with default
846 parameters, using random, matched regions as background. Merged bigwig tracks for
847 visualisation were created from merged bam files from all replicates using the
848 bamCoverage function with scaling factor normalisation and heatmaps and average
849 profiles were plotted with deepTools2[102].
850
851 **Gene ontology analysis**
852 Gene ontology enrichment analysis and pathway enrichment were done using GSEA
853 (v.4.1.0) and MSigDB 7.2[36]. All significant biological processes and pathways had an
854 adj. P value < 0.001.
855
856 **Statistical analyses**
857 The Mann-Whitney-Wilcoxon test was used for 2-group non-parametric comparisons.
858 Unless otherwise stated, statistical tests were two-sided. Permutation test was used to
859 calculate empirical *P* values, which does not make any assumptions on the underlying
860 distribution of the data. Tumor growth curve data was analysed at ethical end point
861 using a two-tailed unpaired Student's *t*-test. IHC data were analysed by a two-tailed,
862 unpaired Student's *t*-test.
863
864 **Public datasets**
865 ChIP-seq data sets were downloaded from GSE32222 by Ross-Innes *et al.,* 2012[6].
866 ChromHMM data was downloaded from GSE73783 by Achinger-Kawecka *et al*.,
867 2020[14].

868 **Data availability**

869 All sequencing data created in this study have been uploaded to the Gene Expression
870 Omnibus (GEO; https://www.ncbi.nlm.nih.gov/geo/) and are available under primary
871 accession code GSE171074 and GSE216989. Biological material used in this study can
872 be obtained from the authors upon request.

873

874 **Code availability**

875 Python script language (v.2.7.8 and v.3.9.1) and R (v.3.6.3 and v.4.0.3) were used to
876 develop the bioinformatics methods and algorithms in this work. All code for Hi-C and
877 PCHi-C analyses is available within the GitHub repository
878 https://github.com/JoannaAch/PDX_Decitabine_3DEpigenome.

879

880 **Main Figures Legends**

881 **Fig. 1 Decitabine inhibits tumour growth and induces widespread DNA**
882 **hypomethylation.**

883 **(a)** Schematic of models and treatments used in the study and summary of genome-
884 wide assays applied to PDX tumours at end-point.

885 **(b)** Growth of treatment naïve (Vehicle) (100nM PBS, n = 7) and Decitabine-treated
886 (0.5mg/kg, n = 7) Gar15-13 PDX tumours for 35 days or until ethical endpoint. All
887 data are mean ± SEM. *** P value < 0.001.

888 **(c)** Growth of treatment naïve (Vehicle) (100nM PBS, n = 8), and Decitabine-treated
889 (0.5mg/kg, n = 7) HCI-005 PDX tumours for 35 days or until ethical endpoint. All
890 data are mean ± SEM. * *P* value < 0.001.

891 **(d)** Quantification of the proliferation marker Ki-67 at endpoint in Gar15-13 and HCI-
892 005 tumours. Ki-67 proportions from all replicates per treatment were compared by
893 two-tailed T test. * *P* value < 0.001.

894 **(e)** Boxplots showing the distribution of DNA methylation profiles for Gar15-13
895 Vehicle and Decitabine-treated tumours for all EPIC probes across the genome. Black
896 line indicates median ± SD.

897 **(f)** Bar plot showing the association of differentially methylated probes in Gar15-13
898 Decitabine treatment compared to Vehicle across different regulatory regions of the
899 genome as determined by TAMR ChromHMM annotation. Observed over expected
900 fold change enrichment shown. * *P* value < 0.001. The numbers of

901 hypo/hypermethylated probes located within each specific region are presented in the
902 respective column.
903
904 **Fig. 2 Loss of DNA methylation results in de-compaction of chromatin.**
905 **(a)** Scatterplot showing correlation between average eigenvalues per bin in Vehicle
906 and Decitabine-treated Gar15-13 PDX tumours.
907 **(b)** Pie chart showing distribution of different types of switching compartments (A to
908 B; B to A) in Decitabine-treated tumours as compared to Vehicle.
909 **(c)** Boxplot showing DNA methylation levels at compartment regions that switched
910 their assignment from B to A and from A to B in Decitabine-treated (n = 4) and
911 Vehicle (n = 4) PDX tumours. Black line indicates median ± SD.
912 **(d)** Average contact enrichment (saddle plots) between pairs of 50Kb loci arranged by
913 their PC1 eigenvector in Vehicle and Decitabine-treated tumours. Average data from
914 n = 3 Hi-C replicates for Vehicle and Decitabine shown. The numbers at the centre of
915 the heatmaps indicate compartment strength calculated as the log2 transformed ratio
916 of (A–A + B–B)/ (A–B + B–A) using the mean values.
917 **(e)** Difference in Hi-C data between Vehicle and Decitabine treatments. Saddle plots
918 were calculated using the averaged PC1 obtained from Vehicle (n = 3) and
919 Decitabine-treated (n = 3) tumours.
920 **(f)** Density plot of insulation scores calculated in Vehicle and Decitabine-treated
921 tumours.
922 **(g)** Number of TADs identified in Vehicle (n = 3) and Decitabine-treated (n = 3) PDX
923 tumours.
924 **(h)** Venn diagram showing overlap between TAD boundaries identified in Vehicle
925 and Decitabine-treated tumours.
926 **(i)** Snapshot of region on chromosome 1, showing Vehicle (top panel) and
927 Decitabine-treated tumour Hi-C matrixes (bottom panel), demonstrating loss of a
928 TAD in Decitabine-treated samples (indicated with an arrow), concomitant with
929 decreased insulation at that region. Merged Hi-C data from replicates (n = 3 each)
930 shown at 10Kb resolution.

931 **Fig. 3 Loss of DNA methylation rewires 3D enhancer-promoter interactions.**
932 **(a)** Browser snapshot of interactions landscape at the *PRR5L* gene demonstrating
933 increased coverage of promoter-anchored interactions in PCHi-C at 1.5Kb resolution
934 compared to Hi-C at 10Kb resolution. Bait and other end (OE) regions marked for
935 illustrative purposes.
936 **(b)** ChromHMM (TAMR) annotation of CHiCAGO significant interaction bait
937 (promoter) and other end (OEs) regions (putative enhancers) in Decitabine-treated
938 and Vehicle samples (* *P* value < 0.001)
939 **(c)** Overlap between promoter bait and other end (OE) enhancer regions for
940 CHiCAGO significant interactions in Vehicle and Decitabine-treated tumours.
941 Merged data across replicates shown.
942 **(d)** Violin plots showing the log10 genomic distance of promoter interactions whose
943 enhancer OEs are gained, maintained or lost following Decitabine treatment. *P* value
944 < 0.0001, Wilcoxon test. Merged data across replicates shown.
945 **(e)** Average number of enhancer OE interactions per promoter bait. Error bars
946 indicate the interquartile range. *P* value Wilcoxon test.
947 **(f)** Scatterplot showing number of enhancer OE interactions per promoter bait for
948 each CHiCAGO significant promoter-anchored interaction in Vehicle and Decitabine-
949 treated tumours. Merged data across replicates shown.
950 **(g)** Percent of overlap of promoter baits and enhancer OEs that are either gained or
951 lost in Decitabine with compartment that switch with Decitabine (A to B or B to A).
952
953 **Fig. 4 Rewired 3D chromatin interactions align with altered transcription**
954 **(a)** Normalized enrichment scores (NES) for signature gene sets representing
955 differentially expressed genes in RNA-seq data from Gar15-13 PDX tumours treated
956 with Decitabine compared to Vehicle (n = 4; FDR < 0.05)
957 **(b)** Volcano plot showing Decitabine *vs.* Vehicle differential expression of genes that
958 are located at enhancer-promoter interactions gained with Decitabine treatment.
959 **(c)** Transcription factor motifs significantly enriched at promoter-interacting enhancers
960 (enhancer OEs) gained with Decitabine treatment. Only motifs with FDR < 0.05 are
961 shown.
962 **(d)** Overlap of consensus ER cistromes in Vehicle and Decitabine-treated Gar15-13
963 PDX tumours (n = 4 each). Heatmaps indicate ER ChIP-seq signal intensity at ER
964 binding sites gained and lost in Decitabine compared to Vehicle-treated tumours.

965 **(e)** Average signal intensity of ER ChIP-seq binding (Gar15-13 Vehicle and
966 Decitabine tumours) at gained and lost ER binding sites with Decitabine treatment.
967 **(f)** ChromHMM (TAMR) annotation (*P value < 0.001) of ER binding sites gained
968 with Decitabine treatment compared to matched random regions across the genome.
969 Size of the overlap is presented in the respective column.
970 **(g)** Transcriptions factor motifs enriched at ER binding sites gained with Decitabine
971 treatment compared to matched random regions generated from ERE binding motifs
972 across the genome.
973 **(h)** Heatmap showing DNA methylation levels (β-values) at gained ER binding sites
974 in Decitabine-treated (n = 4) and Vehicle (n = 4) PDX tumours.
975 **(i)** Browser snapshot of ER ChIP-seq together with EPIC DNA methylation (Vehicle
976 and Decitabine treatment, n = 4 each) showing gain of ER binding and loss of DNA
977 methylation at an enhancer region of ER target gene *ANKRD2*.
978
979 **Fig. 5 Rewired ER-bound interactions are associated with activation of ER**
980 **target genes.**
981 **(a)** Observed/expected fold change enrichment of gained enhancer OEs for ER
982 binding gained and lost following Decitabine treatment. * P value < 0.0001.
983 **(b)** Average ER ChIP-seq signal intensity (Gar15-13 Vehicle and Decitabine-treated
984 tumours) at ER binding sites located at DNA hypomethylation-induced enhancer OEs.
985 **(c)** Heatmap showing expression of genes connected to gained ER-mediated enhancer
986 OEs in Vehicle and Decitabine-treated tumours.
987 **(d)** Browser snapshots showing the promoter-anchored interactions at the *SPATA18*
988 gene, together with the average ER ChIP-seq signal, EPIC DNA methylation and
989 ChromHMM track. Merged replicate data shown (n = 4 each). In Decitabine-treated
990 tumours, the *SPATA18* promoter displays an increased number of interactions with an
991 upstream enhancer region, which gains ER binding with Decitabine treatment,
992 concomitant with loss of DNA methylation. Expression of the *SPATA18* gene was
993 significantly upregulated in Decitabine-treated tumours (shown in Extended Data Fig.
994 5a).
995 **(e)** Browser snapshots showing promoter-anchored interactions at the *SCUBE2* ER
996 target gene, together with ER ChIP-seq, EPIC DNA methylation and ChromHMM
997 track. Merged replicate data shown (n = 4 each). In Decitabine-treated tumours, the
998 *SCUBE2* promoter displays additional interactions with a distal enhancer, which gains

999 ER binding with Decitabine treatment. Expression of the *SCUBE2* gene was
1000 significantly upregulated in Decitabine-treated tumours (shown in Extended Data Fig.
1001 5b).
1002 **(f)** Browser snapshots showing promoter-anchored interactions at the *B4GALT1* ER
1003 target gene, together with ER ChIP-seq, EPIC DNA methylation and ChromHMM
1004 track. Merged replicate data shown (n = 4 each). In Decitabine-treated tumours, the
1005 *B4GALT1* promoter displays additional long-range interactions with a distal enhancer,
1006 which gains ER binding with Decitabine treatment. Expression of the *B4GALT1* gene
1007 was significantly upregulated in Decitabine-treated tumours (shown in Extended Data
1008 Fig. 5c).
1009
1010 **Fig. 6 Dynamics between DNA methylation and 3D chromatin interactions**
1011 **(a)** Experimental design for the Decitabine treatment loss and DNA methylation
1012 "rescue" time-course study in TAMR cell line.
1013 **(b)** Boxplots showing the distribution of DNA methylation profiles for Control
1014 (Control Early and Control Late; n = 2 replicates), Decitabine-treated (Day 7
1015 Decitabine; n = 2) and 28 days post-Decitabine treatment (Decitabine Recovery; n =
1016 2) TAMR cells for all EPIC probes across the genome. Black line indicates median ±
1017 SD.
1018 **(c)** Bar plot showing the association of differentially methylated probes in Day 7
1019 Decitabine treatment TAMR cells compared to Control Early TAMR cells across
1020 different regulatory regions of the genome as determined by TAMR ChromHMM
1021 annotation. Observed over expected fold change enrichment shown. * *P* value <
1022 0.001. The numbers of hypo/hypermethylated probes located within each specific
1023 region are presented in the respective column.
1024 **(d)** Observed/expected fold change enrichment of Day 7 Decitabine hypomethylated
1025 DMRs (as compared to Control Early) and Decitabine Recovery re-methylated DMRs
1026 (as compared to Day 7 Decitabine) for ER binding in TAMR cells. * *P* value <
1027 0.0001.
1028 **(e)** Bar plot showing the association of EPIC probes that become re-methylated in
1029 Decitabine Recovery TAMR cells compared to Day 7 Decitabine cells across
1030 different regulatory regions of the genome as determined by TAMR ChromHMM
1031 annotation. Observed over expected fold change enrichment shown. * *P* value <

1032 0.001. The numbers of re-methylated probes located within each specific region are
1033 presented in the respective column.
1034 **(f)** Scatterplot showing number of enhancer OE interactions per promoter bait for
1035 each CHiCAGO significant promoter-anchored interaction in Day 7 Decitabine and
1036 Control Early TAMR cells. Merged data across replicates shown.
1037 **(g)** Scatterplot showing number of enhancer OE interactions per promoter bait for
1038 each CHiCAGO significant promoter-anchored interaction in Decitabine Recovery
1039 and Control Late TAMR cells. Merged data across replicates shown.
1040 **(h)** Overlap between other end (OE) enhancer regions for CHiCAGO significant
1041 interactions between Day 7 Decitabine and Control Early samples (left panel) and
1042 Decitabine Recovery and Control Late samples (right panel). Below panel shows
1043 overlap between gained interactions in Day 7 Decitabine *vs.* Control Early and
1044 Decitabine Recovery vs. Control Late, demonstrating the number of "recovered" and
1045 "non-recovered" interactions. Merged data across replicates shown.
1046
1047 **Fig. 7 Dynamics of altered ER-bound 3D chromatin interactions on gene**
1048 **transcription**
1049 **(a)** Volcano plot showing Day 7 Decitabine *vs.* Control Early differential expression
1050 of genes involved in gained differential interactions in Day 7 Decitabine-treated
1051 TAMRs. Genes included in representative examples are labelled.
1052 **(b)** Volcano plot showing Decitabine Recovery *vs.* Control Late differential
1053 expression of genes involved in "recovered" differential interactions in Decitabine
1054 Recovery TAMRs. Genes included in representative examples are labelled.
1055 **(c)** Browser snapshots showing promoter-anchored interactions at the *SPATA18* ER
1056 target gene. Data from Gar15-13 PDX model (ER ChIP-seq, EPIC and PCHi-C) has
1057 been overlayed with TAMR cell line data (EPIC and PCHi-C) together with ER ChIP-
1058 seq for MCF7/TAMR cell lines (Ross-Innes *et al.,* 2012) and ChromHMM track.
1059 Merged replicate data shown (n = 4 each for Gar15-13 and n = 2 for TAMRs). In
1060 Decitabine-treated PDX tumours and TAMRs (Day 7 Decitabine), the *SPATA18*
1061 promoter displays an increased number of interactions with an upstream enhancer
1062 region, which gains ER binding with Decitabine treatment in PDXs, concomitant with
1063 loss of DNA methylation in both PDXs and TAMRs. These ectopic chromatin
1064 interactions are lost after 28 days of recovery with partial recovery of DNA
1065 methylation at that locus. Expression of the *SPATA18* gene was significantly

1066 upregulated in Day 7 Decitabine-treated TAMRs and suppressed in Decitabine
1067 Recovery TAMRs. Expression of the *SPATA18* gene was significantly upregulated in
1068 Decitabine-treated *vs.* Vehicle PDXs.
1069 **(d)** Browser snapshots showing promoter-anchored interactions at the *B4GALT1* ER
1070 target gene. Data from Gar15-13 PDX model (ER ChIP-seq, EPIC and PCHi-C) has
1071 been overlayed with TAMR cell line data (EPIC and PCHi-C) together with ER ChIP-
1072 seq for MCF7/TAMR cell lines (Ross-Innes *et al.,* 2012) and ChromHMM track.
1073 Merged replicate data shown (n = 4 each for Gar15-13 and n = 2 for TAMRs). In
1074 Decitabine-treated PDX tumours and TAMRs (Day 7 Decitabine), the *B4GALT1*
1075 promoter displays an increased number of long-range interactions with a distal
1076 enhancer region, which gains ER binding with Decitabine treatment in PDXs,
1077 concomitant with loss of DNA methylation in both PDXs and TAMRs. These ectopic
1078 chromatin interactions are partially reversed after 28 days of recovery with recovery
1079 of DNA methylation at that enhancer locus. *B4GALT1* expression increased in Day 7
1080 Decitabine-treated TAMRs compared to Control Early samples and was restored in
1081 Decitabine Recovery TAMRs. Expression of the *B4GALT1* gene was significantly
1082 upregulated in Decitabine-treated *vs.* Vehicle PDXs. In TAMRs
1083
1084 **Fig. 8 Model of Decitabine-induced 3D epigenome remodelling and suppression**
1085 **of tumour growth**
1086 Proposed model of tumour growth suppression induced by epigenetic therapy with
1087 Decitabine *via* DNA hypomethylation and subsequent rewiring of ER-bound 3D
1088 enhancer-promoter interactions resulting in activation of specific ER target genes.

Acknowledgments

We thank members of the Clark Laboratory for helpful discussions and careful reading of the manuscript. We thank Arima Genomics Inc. for advice with performing Hi-C and Promoter Capture Hi-C in snap-frozen tumour tissues. S.J.C. is a National Health and Medical Research Council (NHMRC) Senior Principal Research Fellow #1063559. J.A-K. is a National Breast Cancer Foundation (NBCF) Mavis Robertson Fellow #IIRS-21-047. E.L. is a NBCF Endowed Chair. T.E.H. is an NBCF Fellow #IIRS-19-009. C.S. is an NBCF Fellow IIRS-18-137. Q.D. is a NHMRC Investigator Grant recipient #1177792. J.M.W.G is supported by a Breast Cancer Now Fellowship and the Tenovus Cancer Charity. This research was supported by the NHMRC Project Grant #1128916 (to S.J.C), Movember & National Breast Cancer Foundation Collaboration Initiative grant (MNBCF-17-012 to T.E.H., E.L., S.J.C.) and the Cancer Council NSW grants RG16-09 (to S.J.C) and RG20-04 (to J.A-K.). Research funding (to S.J.C.) was provided by Van Andel Institute through the Van Andel Institute – Stand Up To Cancer Epigenetics Dream Team. Stand Up To Cancer is a division of the Entertainment Industry Foundation, administered by AACR. The contents of the published material are solely the responsibility of the administering institution and individual authors and do not reflect the views of the NHMRC.

Author Contributions

Conception (S.J.C., C.S., J.A-K) and Experimental Design: J.A-K., K-M.C., N.P., T.E.H., E.L., C.S. and S.J.C. Methodology and Data Acquisition: J.A-K., K-M.C., N.P., E.C., A.Y., A.W., G.L.L., A.S., E.W., J.G., A.K., S.A., J.S. Data Analysis: J.A-K., E.C., H.H.M., B.M., S.C. and Q.D. Data Interpretation: J.A-K., K-M.C., N.P., E.C., E.C.C., Q.D., T.E.H., E.L., C.S. and S.J.C. Funding Acquisition: J.A-K., T.E.H., E.L. and S.J.C. Manuscript Writing: J.A-K. and S.J.C. with input from all authors.

Ethics declarations

A.S. is an employee of Arima Genomics, Inc. Other authors declare no competing interests.

1122 **References**

1123

1124 1. Farcas, A.M., Nagarajan, S., Cosulich, S. & Carroll, J.S. Genome-Wide
1125 Estrogen Receptor Activity in Breast Cancer. *Endocrinology* **162**(2021).

1126 2. Musgrove, E.A. & Sutherland, R.L. Biological determinants of endocrine
1127 resistance in breast cancer. *Nat Rev Cancer* **9**, 631-43 (2009).

1128 3. Ali, S. & Coombes, R.C. Endocrine-responsive breast cancer and strategies for
1129 combating resistance. *Nat Rev Cancer* **2**, 101-12 (2002).

1130 4. Garcia-Martinez, L., Zhang, Y., Nakata, Y., Chan, H.L. & Morey, L. Epigenetic
1131 mechanisms in breast cancer therapy and resistance. *Nat Commun* **12**, 1786
1132 (2021).

1133 5. Dimitrakopoulos, F.I., Kottorou, A. & Tzezou, A. Endocrine resistance and
1134 epigenetic reprogramming in estrogen receptor positive breast cancer. *Cancer*
1135 *Lett* **517**, 55-65 (2021).

1136 6. Ross-Innes, C.S. *et al.* Differential oestrogen receptor binding is associated with
1137 clinical outcome in breast cancer. *Nature* **481**, 389-93 (2012).

1138 7. Lupien, M. *et al.* Growth factor stimulation induces a distinct ER(alpha)
1139 cistrome underlying breast cancer endocrine resistance. *Genes Dev* **24**, 2219-27
1140 (2010).

1141 8. Achinger-Kawecka, J. & Clark, S.J. Disruption of the 3D cancer genome
1142 blueprint. *Epigenomics* **9**, 47-55 (2017).

1143 9. Taberlay, P.C. *et al.* Three-dimensional disorganization of the cancer genome
1144 occurs coincident with long-range genetic and epigenetic alterations. *Genome*
1145 *Res* **26**, 719-31 (2016).

1146 10. Rhie, S.K. *et al.* A high-resolution 3D epigenomic map reveals insights into the
1147 creation of the prostate cancer transcriptome. *Nat Commun* **10**, 4154 (2019).

1148 11. Barutcu, A.R. *et al.* RUNX1 contributes to higher-order chromatin organization
1149 and gene regulation in breast cancer cells. *Biochim Biophys Acta* **1859**, 1389-
1150 1397 (2016).

1151 12. Barutcu, A.R. *et al.* SMARCA4 regulates gene expression and higher-order
1152 chromatin structure in proliferating mammary epithelial cells. *Genome Res* **26**,
1153 1188-201 (2016).

1154 13. Barutcu, A.R. *et al.* Chromatin interaction analysis reveals changes in small
1155 chromosome and telomere clustering between epithelial and breast cancer cells.
1156 *Genome Biol* **16**, 214 (2015).

1157 14. Achinger-Kawecka, J. *et al.* Epigenetic reprogramming at estrogen-receptor
1158 binding sites alters 3D chromatin landscape in endocrine-resistant breast cancer.
1159 *Nat Commun* **11**, 320 (2020).

1160 15. Zhou, Y. *et al.* Temporal dynamic reorganization of 3D chromatin architecture
1161 in hormone-induced breast cancer and endocrine resistance. *Nat Commun* **10**,
1162 1522 (2019).

1163 16. Flavahan, W.A. *et al.* Insulator dysfunction and oncogene activation in IDH
1164 mutant gliomas. *Nature* **529**, 110-4 (2016).

1165 17. Kloetgen, A. *et al.* Three-dimensional chromatin landscapes in T cell acute
1166 lymphoblastic leukemia. *Nat Genet* **52**, 388-400 (2020).

1167 18. Vilarrasa-Blasi, R. *et al.* Dynamics of genome architecture and chromatin
1168 function during human B cell differentiation and neoplastic transformation. *Nat*
1169 *Commun* **12**, 651 (2021).

1170 19. Corces, M.R. & Corces, V.G. The three-dimensional cancer genome. *Curr Opin*
1171 *Genet Dev* **36**, 1-7 (2016).

1172 20. Yang, Y. *et al.* The 3D Genomic Landscape of Differential Response to
1173 EGFR/HER2 Inhibition in Endocrine-Resistant Breast Cancer Cells. *Biochim*
1174 *Biophys Acta Gene Regul Mech*, 194631 (2020).

1175 21. Bates, S.E. Epigenetic Therapies for Cancer. *N Engl J Med* **383**, 650-663 (2020).

1176 22. Pandiyan, K. *et al.* Functional DNA demethylation is accompanied by
1177 chromatin accessibility. *Nucleic Acids Res* **41**, 3973-85 (2013).

1178 23. Yang, X. *et al.* Gene body methylation can alter gene expression and is a
1179 therapeutic target in cancer. *Cancer Cell* **26**, 577-90 (2014).

1180 24. Mehdipour, P. *et al.* Epigenetic therapy induces transcription of inverted SINEs
1181 and ADAR1 dependency. *Nature* **588**, 169-+ (2020).

1182 25. Roulois, D. *et al.* DNA-Demethylating Agents Target Colorectal Cancer Cells
1183 by Inducing Viral Mimicry by Endogenous Transcripts. *Cell* **162**, 961-973
1184 (2015).

1185 26. Loo Yau, H. *et al.* DNA hypomethylating agents increase activation and
1186 cytolytic activity of CD8(+) T cells. *Mol Cell* (2021).

1187 27. Cazet, A.S. *et al.* Targeting stromal remodeling and cancer stem cell plasticity
1188 overcomes chemoresistance in triple negative breast cancer. *Nat Commun* **9**,
1189 2897 (2018).

1190 28. Chia, K. *et al.* Non-canonical AR activity facilitates endocrine resistance in
1191 breast cancer. *Endocr Relat Cancer* **26**, 251-264 (2019).

1192 29. Portman, N. *et al.* MDM2 inhibition in combination with endocrine therapy and
1193 CDK4/6 inhibition for the treatment of ER-positive breast cancer. *Breast*
1194 *Cancer Research* **22**(2020).

1195 30. Hickey, T.E. *et al.* The androgen receptor is a tumor suppressor in estrogen
1196 receptor-positive breast cancer. *Nat Med* **27**, 310-320 (2021).

1197 31. DeRose, Y.S. *et al.* Tumor grafts derived from women with breast cancer
1198 authentically reflect tumor pathology, growth, metastasis and disease outcomes.
1199 *Nat Med* **17**, 1514-20 (2011).

1200 32. Zheng, Y. *et al.* Prediction of genome-wide DNA methylation in repetitive
1201 elements. *Nucleic Acids Res* **45**, 8697-8711 (2017).

1202 33. Lieberman-Aiden, E. *et al.* Comprehensive mapping of long-range interactions
1203 reveals folding principles of the human genome. *Science* **326**, 289-93 (2009).

1204 34. Cairns, J. *et al.* CHiCAGO: robust detection of DNA looping interactions in
1205 Capture Hi-C data. *Genome Biol* **17**, 127 (2016).

1206 35. Cairns, J., Orchard, W.R., Malysheva, V. & Spivakov, M. Chicdiff: a
1207 computational pipeline for detecting differential chromosomal interactions in
1208 Capture Hi-C data. *Bioinformatics* **35**, 4764-4766 (2019).

1209 36. Subramanian, A. *et al.* Gene set enrichment analysis: a knowledge-based
1210 approach for interpreting genome-wide expression profiles. *Proc Natl Acad Sci*
1211 *U S A* **102**, 15545-50 (2005).

1212 37. Zuin, J. *et al.* Nonlinear control of transcription through enhancer-promoter
1213 interactions. *bioRxiv* (2021).

1214 38. Zhu, I., Song, W., Ovcharenko, I. & Landsman, D. A model of active
1215 transcription hubs that unifies the roles of active promoters and enhancers.
1216 *Nucleic Acids Res* (2021).

1217 39. Fullwood, M.J. *et al.* An oestrogen-receptor-alpha-bound human chromatin
1218 interactome. *Nature* **462**, 58-64 (2009).

1219 40. Nye, A.C. *et al.* Alteration of large-scale chromatin structure by estrogen
1220 receptor. *Mol Cell Biol* **22**, 3437-49 (2002).

1221 41. Rafique, S., Thomas, J.S., Sproul, D. & Bickmore, W.A. Estrogen-induced
1222 chromatin decondensation and nuclear re-organization linked to regional
1223 epigenetic regulation in breast cancer. *Genome Biol* **16**, 145 (2015).

1224 42. Yin, Y. *et al.* Impact of cytosine methylation on DNA binding specificities of
1225 human transcription factors. *Science* **356**(2017).

1226 43. Gee, J.M. *et al.* Antihormone induced compensatory signalling in breast cancer:
1227 an adverse event in the development of endocrine resistance. *Horm Mol Biol*
1228 *Clin Investig* **5**, 67-77 (2011).

1229 44. Stone, A. *et al.* DNA methylation of oestrogen-regulated enhancers defines
1230 endocrine sensitivity in breast cancer. *Nat Commun* **6**, 7758 (2015).

1231 45. Achinger-Kawecka, J., Chia, K-M., Portman, N., Campbell, E., Du, Q., Laven-
1232 Law, G., Clifton, S., Milioli, H.H., Schmitt, A., Wong, E., Hickey, T., Lim, E.,
1233 Stirzaker, C., Clark, S.J. Epigenetic therapy suppresses tumour growth by
1234 rewiring ER-mediated long-range chromatin interactions in ER+ endocrine-
1235 resistant breast cancer. *bioRxiv* (2021).

1236 46. Linnekamp, J.F., Butter, R., Spijker, R., Medema, J.P. & van Laarhoven,
1237 H.W.M. Clinical and biological effects of demethylating agents on solid
1238 tumours - A systematic review. *Cancer Treat Rev* **54**, 10-23 (2017).

1239 47. Oronsky, B., Oronsky, N., Knox, S., Fanger, G. & Scicinski, J. Episensitization:
1240 therapeutic tumor resensitization by epigenetic agents: a review and
1241 reassessment. *Anticancer Agents Med Chem* **14**, 1121-7 (2014).

1242 48. Tsai, H.C. *et al.* Transient Low Doses of DNA-Demethylating Agents Exert
1243 Durable Antitumor Effects on Hematological and Epithelial Tumor Cells.
1244 *Cancer Cell* **21**, 430-446 (2012).

1245 49. Lu, Z. *et al.* Epigenetic therapy inhibits metastases by disrupting premetastatic
1246 niches. *Nature* **579**, 284-290 (2020).

1247 50. Yu, J. *et al.* DNA methyltransferase expression in triple-negative breast cancer
1248 predicts sensitivity to decitabine. *J Clin Invest* **128**, 2376-2388 (2018).

1249 51. Dahn, M.L. *et al.* Decitabine Response in Breast Cancer Requires Efficient
1250 Drug Processing and Is Not Limited by Multidrug Resistance. *Mol Cancer Ther*
1251 **19**, 1110-1122 (2020).

1252 52. de Cubas, A.A. *et al.* DNA hypomethylation promotes transposable element
1253 expression and activation of immune signaling in renal cell cancer. *JCI Insight*
1254 **5**(2020).

1255 53. Johnstone, S.E. *et al.* Large-Scale Topological Changes Restrain Malignant
1256 Progression in Colorectal Cancer. *Cell* **182**, 1474-1489 e23 (2020).

1257 54. Buitrago, D. *et al.* Impact of DNA methylation on 3D genome structure. *Nat*
1258 *Commun* **12**, 3243 (2021).

1259 55. Flavahan, W.A. *et al.* Altered chromosomal topology drives oncogenic
1260 programs in SDH-deficient GISTs. *Nature* **575**, 229-233 (2019).

1261 56. Xu, J. *et al.* Subtype-specific 3D genome alteration in acute myeloid leukaemia.
1262 *Nature* (2022).

1263 57. Lee, D.S. *et al.* Simultaneous profiling of 3D genome structure and DNA
1264 methylation in single human cells. *Nat Methods* **16**, 999-1006 (2019).

1265 58. Bell, A.C. & Felsenfeld, G. Methylation of a CTCF-dependent boundary
1266 controls imprinted expression of the Igf2 gene. *Nature* **405**, 482-5 (2000).

1267 59. Hark, A.T. *et al.* CTCF mediates methylation-sensitive enhancer-blocking
1268 activity at the H19/Igf2 locus. *Nature* **405**, 486-9 (2000).

1269 60. Maurano, M.T. *et al.* Role of DNA Methylation in Modulating Transcription
1270 Factor Occupancy. *Cell Rep* **12**, 1184-95 (2015).

1271 61. Ahmed, M. *et al.* CRISPRi screens reveal a DNA methylation-mediated 3D
1272 genome dependent causal mechanism in prostate cancer. *Nat Commun* **12**, 1781
1273 (2021).

1274 62. Du, Q. *et al.* DNA methylation is required to maintain DNA replication timing
1275 precision and 3D genome integrity. *bioRxiv* (2020).

1276 63. McLaughlin, K. *et al.* DNA Methylation Directs Polycomb-Dependent 3D
1277 Genome Re-organization in Naive Pluripotency. *Cell Rep* **29**, 1974-1985 e6
1278 (2019).

1279 64. Broome, R. *et al.* TET2 is a component of the estrogen receptor complex and
1280 controls 5mC to 5hmC conversion at estrogen receptor cis-regulatory regions.
1281 *Cell Rep* **34**, 108776 (2021).

1282 65. Bi, M. *et al.* Enhancer reprogramming driven by high-order assemblies of
1283 transcription factors promotes phenotypic plasticity and breast cancer endocrine
1284 resistance. *Nat Cell Biol* **22**, 701-715 (2020).

1285 66. Nagarajan, S. *et al.* ARID1A influences HDAC1/BRD4 activity, intrinsic
1286 proliferative capacity and breast cancer treatment response. *Nat Genet* **52**, 187-
1287 197 (2020).

1288 67. Schmitt, A.D. *et al.* A Compendium of Chromatin Contact Maps Reveals
1289 Spatially Active Regions in the Human Genome. *Cell Rep* **17**, 2042-2059
1290 (2016).

1291 68. Oudelaar, A.M. *et al.* A revised model for promoter competition based on multi-
1292 way chromatin interactions at the alpha-globin locus. *Nat Commun* **10**, 5412
1293 (2019).

1294 69. Thomas, H.F. *et al.* Temporal dissection of an enhancer cluster reveals distinct
1295 temporal and functional contributions of individual elements. *Mol Cell* (2021).

1296 70. DeRose, Y.S. *et al.* Tumor grafts derived from women with breast cancer
1297 authentically reflect tumor pathology, growth, metastasis and disease outcomes.
1298 *Nature Medicine* **17**, 1514-U227 (2011).

1299 71. Schoenfelder, S. *et al.* The pluripotent regulatory circuitry connecting
1300 promoters to their long-range interacting elements. *Genome Res* **25**, 582-97
1301 (2015).

1302 72. Schoenfelder, S., Javierre, B.M., Furlan-Magaril, M., Wingett, S.W. & Fraser,
1303 P. Promoter Capture Hi-C: High-resolution, Genome-wide Profiling of
1304 Promoter Interactions. *Jove-Journal of Visualized Experiments* (2018).

1305 73. Schoenfelder, S. *et al.* Polycomb repressive complex PRC1 spatially constrains
1306 the mouse embryonic stem cell genome. *Nat Genet* **47**, 1179-1186 (2015).

1307 74. Aryee, M.J. *et al.* Minfi: a flexible and comprehensive Bioconductor package
1308 for the analysis of Infinium DNA methylation microarrays. *Bioinformatics* **30**,
1309 1363-9 (2014).

1310 75. Pidsley, R. *et al.* Critical evaluation of the Illumina MethylationEPIC BeadChip
1311 microarray for whole-genome DNA methylation profiling. *Genome Biol* **17**,
1312 208 (2016).

1313 76. Zhou, W.D., Laird, P.W. & Shen, H. Comprehensive characterization,
1314 annotation and innovative use of Infinium DNA methylation BeadChip probes.
1315 *Nucleic Acids Research* **45**(2017).

1316 77. Ritchie, M.E. *et al.* limma powers differential expression analyses for RNA-
1317 sequencing and microarray studies. *Nucleic Acids Res* **43**, e47 (2015).

1318 78. Peters, T.J. *et al.* De novo identification of differentially methylated regions in
1319 the human genome. *Epigenetics Chromatin* **8**, 6 (2015).

1320 79. Wingett, S.W. & Andrews, S. FastQ Screen: A tool for multi-genome mapping
1321 and quality control. *F1000Res* **7**, 1338 (2018).

1322 80. Conway, T. *et al.* Xenome--a tool for classifying reads from xenograft samples.
1323 *Bioinformatics* **28**, i172-8 (2012).

1324 81. Dozmorov, M.G. *et al.* Chromatin conformation capture (Hi-C) sequencing of
1325 patient-derived xenografts: analysis guidelines. *Gigascience* **10**(2021).

1326 82. Servant, N. *et al.* HiC-Pro: an optimized and flexible pipeline for Hi-C data
1327 processing. *Genome Biology* **16**(2015).

1328 83. Imakaev, M. *et al.* Iterative correction of Hi-C data reveals hallmarks of
1329 chromosome organization. *Nat Methods* **9**, 999-1003 (2012).

1330 84. Wu, P. *et al.* 3D genome of multiple myeloma reveals spatial genome
1331 disorganization associated with copy number variations. *Nat Commun* **8**, 1937
1332 (2017).

1333 85. Durand, N.C. *et al.* Juicer Provides a One-Click System for Analyzing Loop-
1334 Resolution Hi-C Experiments. *Cell Syst* **3**, 95-8 (2016).

1335 86. Durand, N.C. *et al.* Juicebox Provides a Visualization System for Hi-C Contact
1336 Maps with Unlimited Zoom. *Cell Syst* **3**, 99-101 (2016).

1337 87. Zhou, X. *et al.* Exploring long-range genome interactions using the WashU
1338 Epigenome Browser. *Nat Methods* **10**, 375-6 (2013).

1339 88. Kruse, K., Hug, C.B., Hernandez-Rodriguez, B. & Vaquerizas, J.M. TADtool:
1340 visual parameter identification for TAD-calling algorithms. *Bioinformatics* **32**,
1341 3190-3192 (2016).

1342 89. van der Weide, R.H. *et al.* Hi-C Analyses with GENOVA: a case study with
1343 cohesin variants. *bioRxiv* (2021).

1344 90. Wingett, S. *et al.* HiCUP: pipeline for mapping and processing Hi-C data.
1345 *F1000Res* **4**, 1310 (2015).

1346 91. Blighe K, S.R., M Lewis. EnhancedVolcano: Publication-ready volcano plots
1347 with enhanced colouring and labeling. (2018).

1348 92. Dobin, A. *et al.* STAR: ultrafast universal RNA-seq aligner. *Bioinformatics* **29**,
1349 15-21 (2013).

1350 93. Robinson, M.D. & Oshlack, A. A scaling normalization method for differential
1351 expression analysis of RNA-seq data. *Genome Biol* **11**, R25 (2010).

1352 94. Robinson, M.D., McCarthy, D.J. & Smyth, G.K. edgeR: a Bioconductor
1353 package for differential expression analysis of digital gene expression data.
1354 *Bioinformatics* **26**, 139-40 (2010).

1355 95. Jin, Y., Tam, O.H., Paniagua, E. & Hammell, M. TEtranscripts: a package for
1356 including transposable elements in differential expression analysis of RNA-seq
1357 datasets. *Bioinformatics* **31**, 3593-3599 (2015).

1358 96. Love, M.I., Huber, W. & Anders, S. Moderated estimation of fold change and
1359 dispersion for RNA-seq data with DESeq2. *Genome Biology* **15**(2014).

1360 97. Langmead, B., Trapnell, C., Pop, M. & Salzberg, S.L. Ultrafast and memory-
1361 efficient alignment of short DNA sequences to the human genome. *Genome*
1362 *Biol* **10**, R25 (2009).

1363 98. Zhang, Y. *et al.* Model-based analysis of ChIP-Seq (MACS). *Genome Biol* **9**,
1364 R137 (2008).

1365 99. Feng, J.X., Liu, T., Qin, B., Zhang, Y. & Liu, X.S. Identifying ChIP-seq
1366 enrichment using MACS. *Nature Protocols* **7**, 1728-1740 (2012).

1367 100. Heger, A., Webber, C., Goodson, M., Ponting, C.P. & Lunter, G. GAT: a
1368 simulation framework for testing the association of genomic intervals.
1369 *Bioinformatics* **29**, 2046-8 (2013).

1370 101. Yu, G., Wang, L.G. & He, Q.Y. ChIPseeker: an R/Bioconductor package for
1371 ChIP peak annotation, comparison and visualization. *Bioinformatics* **31**, 2382-
1372 3 (2015).

1373 102. Ramirez, F. *et al.* deepTools2: a next generation web server for deep-sequencing
1374 data analysis. *Nucleic Acids Res* **44**, W160-5 (2016).

1375 103. Heinz, S. *et al.* Simple Combinations of Lineage-Determining Transcription
1376 Factors Prime cis-Regulatory Elements Required for Macrophage and B Cell
1377 Identities. *Molecular Cell* **38**, 576-589 (2010).

1378

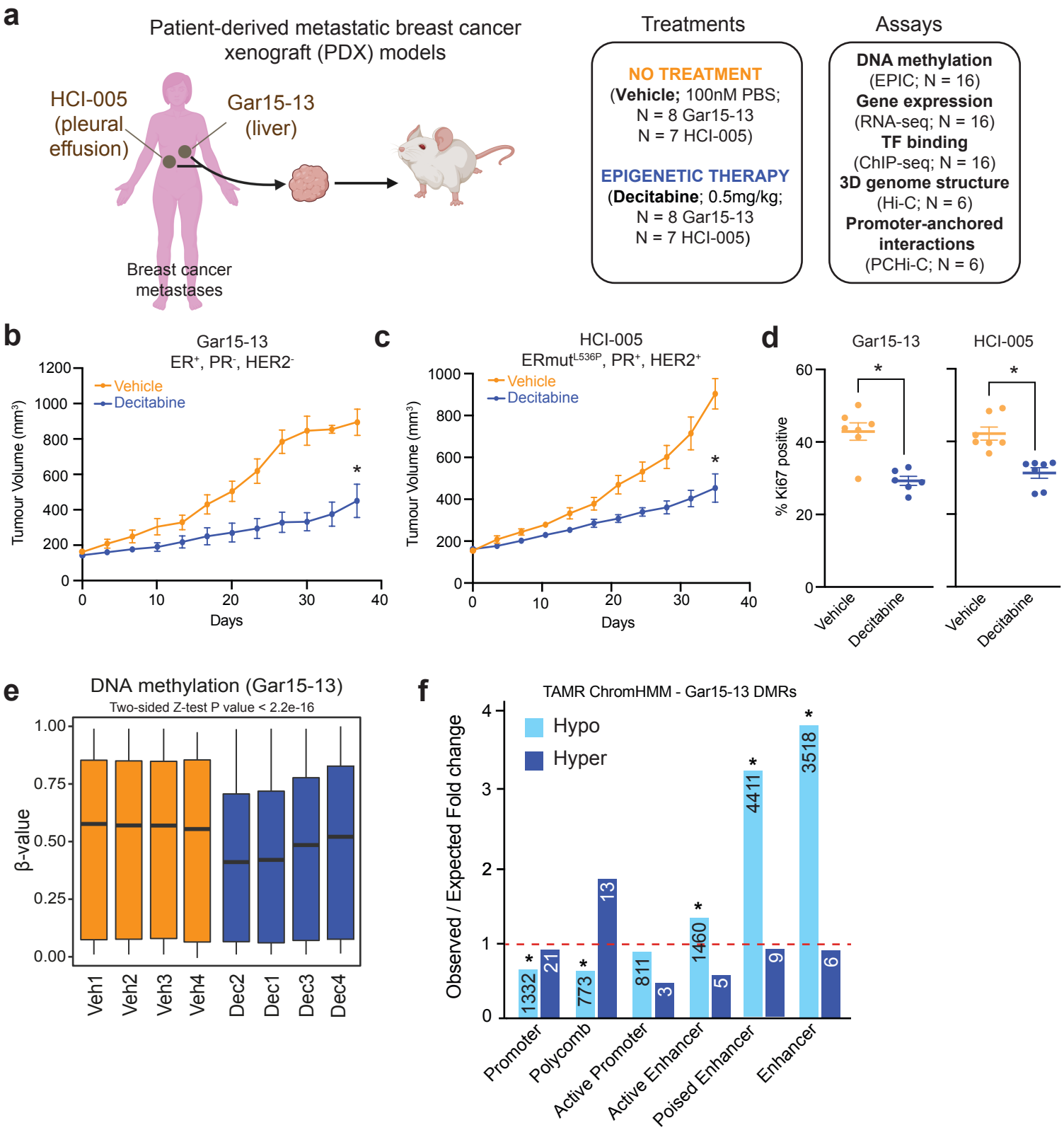
a
Patient-derived metastatic breast cancer xenograft (PDX) models
HCI-005 (pleural effusion)
Gar15-13 (liver)
Breast cancer metastases
Treatments
NO TREATMENT
(Vehicle; 100nM PBS;
N = 8 Gar15-13
N = 7 HCI-005)
EPIGENETIC THERAPY
(Decitabine; 0.5mg/kg;
N = 8 Gar15-13
N = 7 HCI-005)
Assays
DNA methylation
(EPIC; N = 16)
Gene expression
(RNA-seq; N = 16)
TF binding
(ChIP-seq; N = 16)
3D genome structure
(Hi-C; N = 6)
Promoter-anchored interactions
(PCHi-C; N = 6)
b
Gar15-13
ER+, PR-, HER2-
Vehicle
Decitabine
Tumour Volume (mm3)
Days
c
HCI-005
ERmutL536P, PR+, HER2+
Vehicle
Decitabine
Tumour Volume (mm3)
Days
d
Gar15-13
HCI-005
% Ki67 positive
Vehicle
Decitabine
e
DNA methylation (Gar15-13)
Two-sided Z-test P value < 2.2e-16
β-value
Veh1
Veh2
Veh3
Veh4
Dec2
Dec1
Dec3
Dec4
f
TAMR ChromHMM - Gar15-13 DMRs
Hypo
Hyper
Observed / Expected Fold change
1332
21
773
13
811
3
1460
5
4411
9
3518
6
Promoter
Polycomb
Active Promoter
Active Enhancer
Poised Enhancer
Enhancer

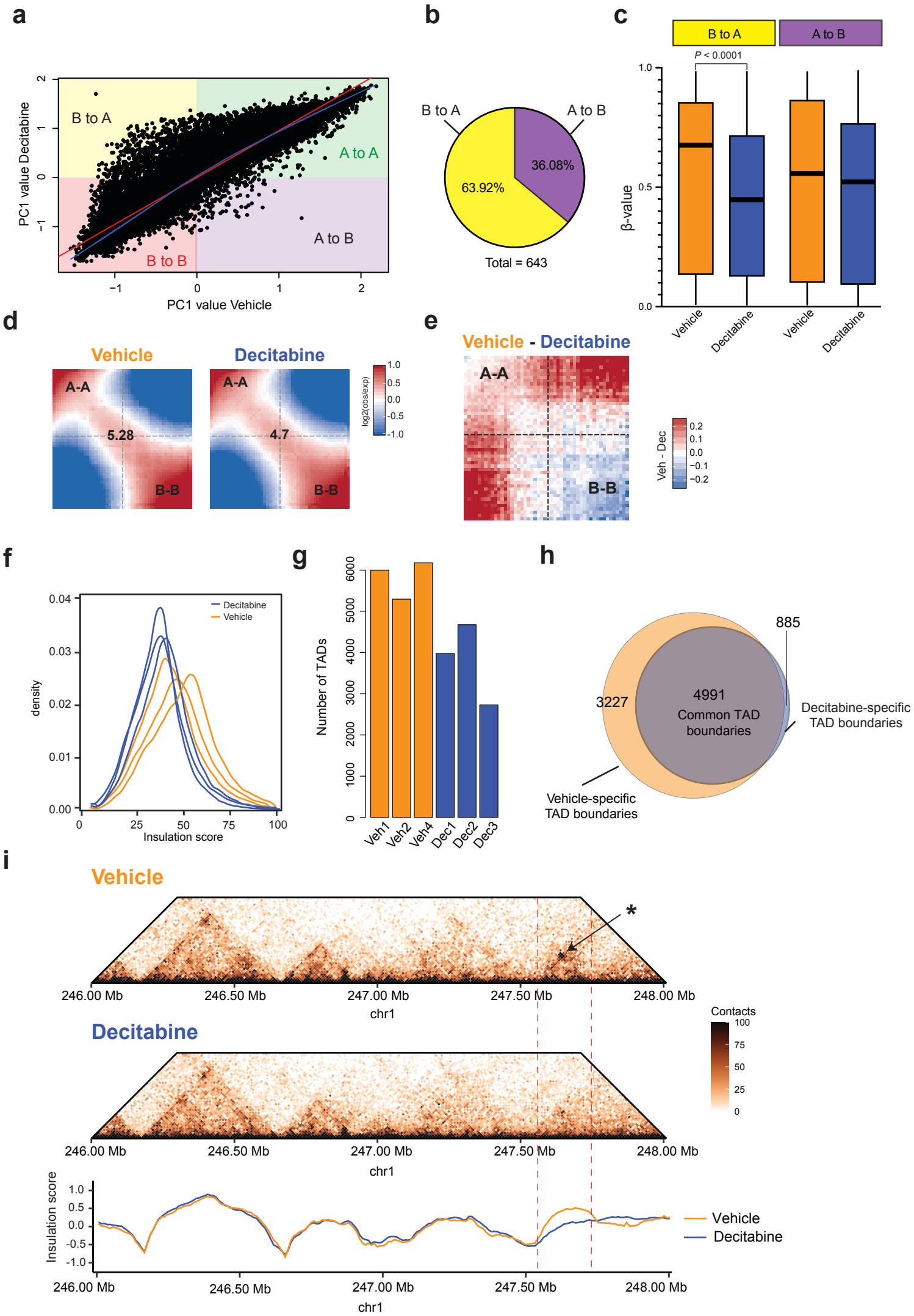
a
B to A
A to A
A to B
B to B
PC1 value Decitabine
PC1 value Vehicle
b
B to A
A to B
36.08%
63.92%
Total = 643
c
B to A
A to B
P < 0.0001
β-value
Vehicle
Decitabine
Vehicle
Decitabine
d
Vehicle
Decitabine
A-A
B-B
5.28
4.7
log2(obs/exp)
e
Vehicle - Decitabine
A-A
B-B
Veh - Dec
f
Decitabine
Vehicle
density
Insulation score
g
Number of TADs
Veh1
Veh2
Veh4
Dec1
Dec2
Dec3
h
885
3227
4991
Common TAD boundaries
Decitabine-specific TAD boundaries
Vehicle-specific TAD boundaries
i
Vehicle
Decitabine
246.00 Mb
246.50 Mb
247.00 Mb
247.50 Mb
248.00 Mb
chr1
Contacts
Insulation score
Vehicle
Decitabine

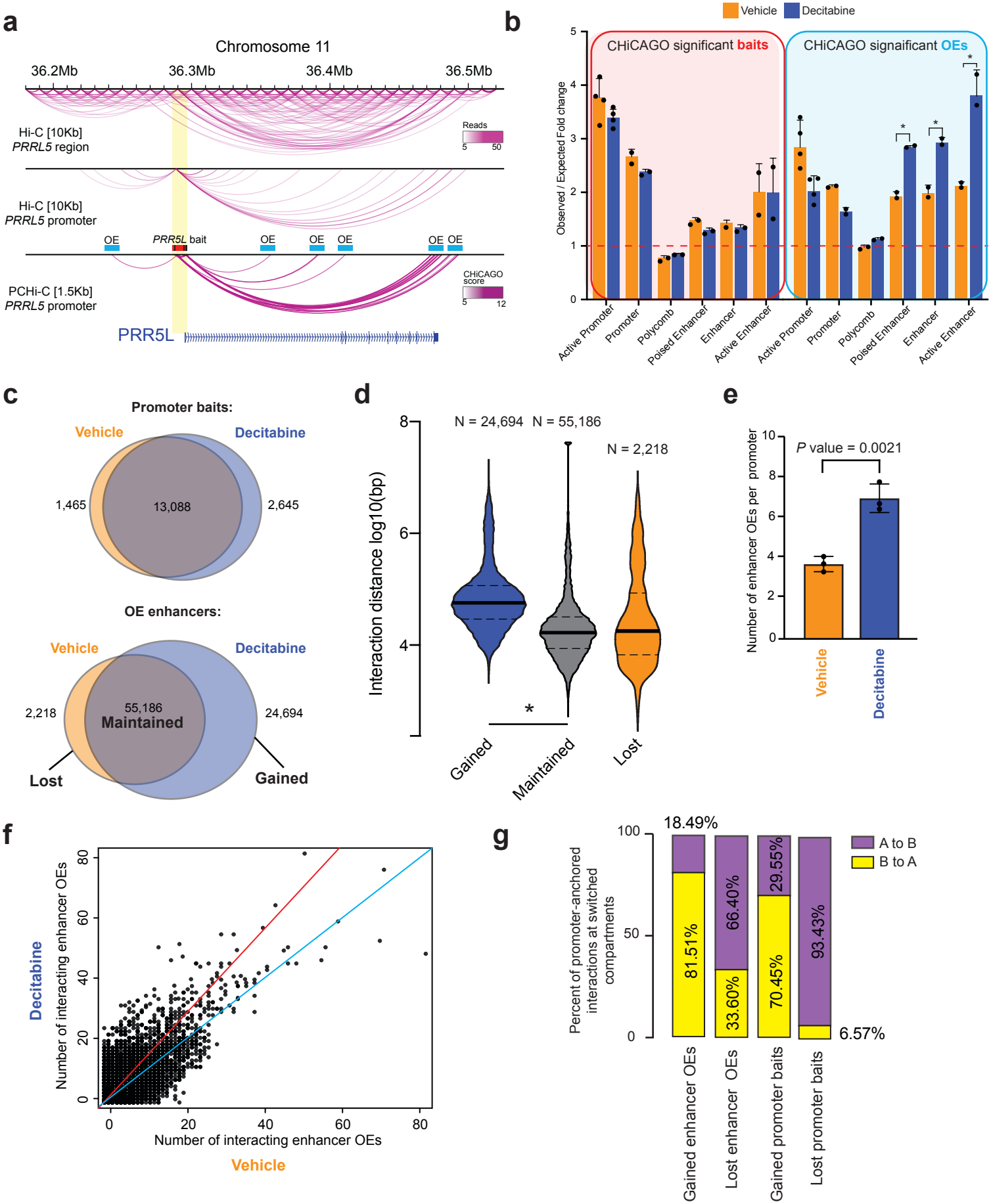
a
Chromosome 11
36.2Mb
36.3Mb
36.4Mb
36.5Mb
Hi-C [10Kb]
PRRL5 region
Reads
5
50
Hi-C [10Kb]
PRRL5 promoter
OE
PRR5L bait
OE
OE
OE
OE
OE
PCHi-C [1.5Kb]
PRRL5 promoter
CHiCAGO score
5
12
PRR5L
b
Vehicle
Decitabine
CHiCAGO significant baits
CHiCAGO signaificant OEs
Observed / Expected Fold change
Active Promoter
Promoter
Polycomb
Poised Enhancer
Enhancer
Active Enhancer
Active Promoter
Promoter
Polycomb
Poised Enhancer
Enhancer
Active Enhancer
c
Promoter baits:
Vehicle
Decitabine
1,465
13,088
2,645
OE enhancers:
Vehicle
Decitabine
2,218
55,186
Maintained
24,694
Lost
Gained
d
N = 24,694
N = 55,186
N = 2,218
Interaction distance log10(bp)
Gained
Maintained
Lost
e
P value = 0.0021
Number of enhancer OEs per promoter
Vehicle
Decitabine
f
Decitabine
Number of interacting enhancer OEs
Number of interacting enhancer OEs
Vehicle
g
Percent of promoter-anchored interactions at switched compartments
18.49%
81.51%
66.40%
33.60%
29.55%
70.45%
93.43%
6.57%
A to B
B to A
Gained enhancer OEs
Lost enhancer OEs
Gained promoter baits
Lost promoter baits

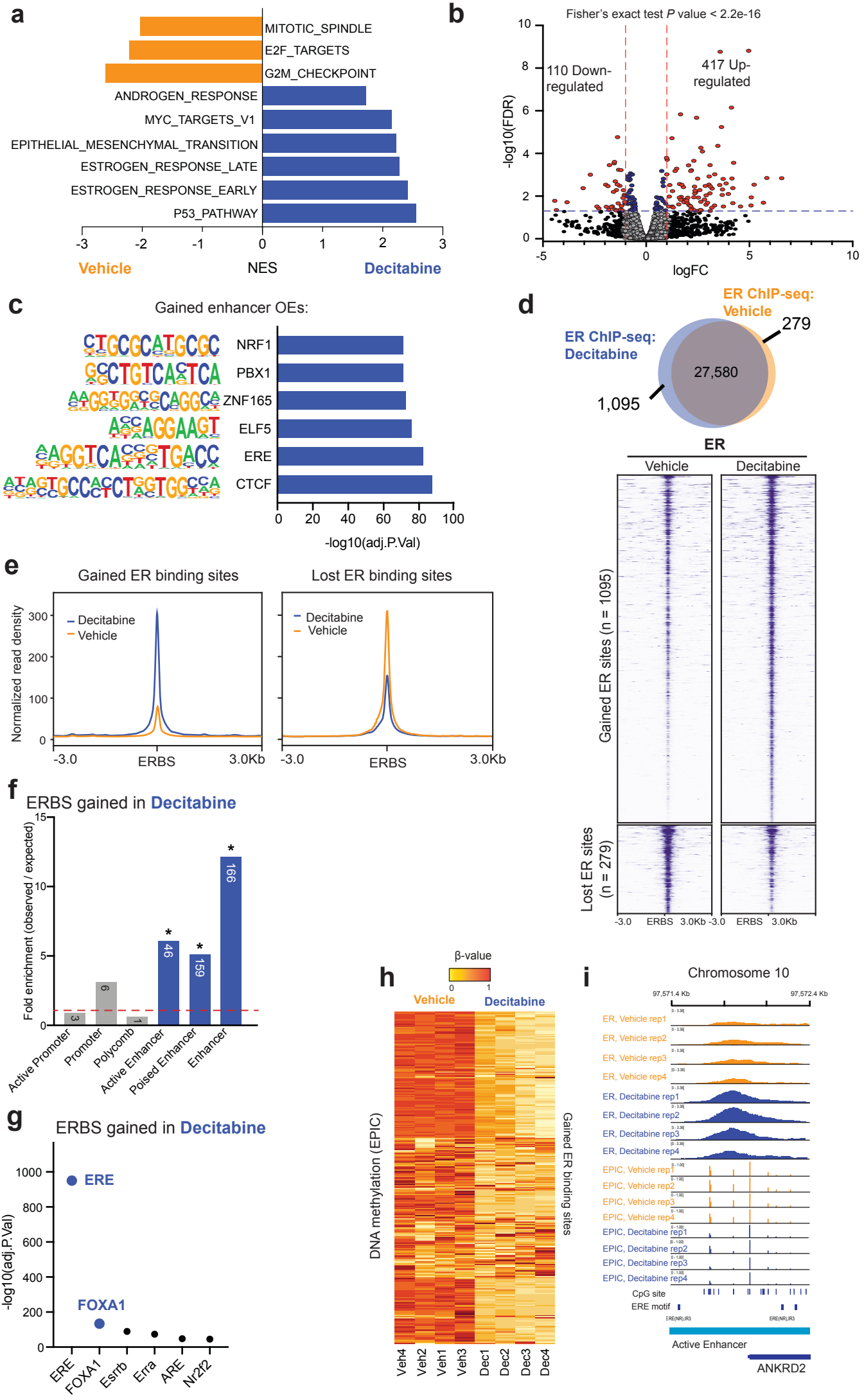
a
MITOTIC_SPINDLE
E2F_TARGETS
G2M_CHECKPOINT
ANDROGEN_RESPONSE
MYC_TARGETS_V1
EPITHELIAL_MESENCHYMAL_TRANSITION
ESTROGEN_RESPONSE_LATE
ESTROGEN_RESPONSE_EARLY
P53_PATHWAY
-3 -2 -1 0 1 2 3
Vehicle
NES
Decitabine
b
Fisher's exact test P value < 2.2e-16
110 Down-regulated
417 Up-regulated
-log10(FDR)
logFC
c
Gained enhancer OEs:
NRF1
PBX1
ZNF165
ELF5
ERE
CTCF
-log10(adj.P.Val)
d
ER ChIP-seq: Vehicle
ER ChIP-seq: Decitabine
279
27,580
1,095
ER
Vehicle
Decitabine
Gained ER sites (n = 1095)
Lost ER sites (n = 279)
-3.0 ERBS 3.0Kb
e
Gained ER binding sites
Lost ER binding sites
Normalized read density
Decitabine
Vehicle
-3.0 ERBS 3.0Kb
f
ERBS gained in Decitabine
Fold enrichment (observed / expected)
3
6
1
46
159
166
Active Promoter
Promoter
Polycomb
Active Enhancer
Poised Enhancer
Enhancer
g
ERBS gained in Decitabine
-log10(adj.P.Val)
ERE
FOXA1
Esrrb
Erra
ARE
Nr2f2
h
β-value
Vehicle
Decitabine
DNA methylation (EPIC)
Gained ER binding sites
Veh4 Veh2 Veh1 Veh3 Dec1 Dec2 Dec3 Dec4
i
Chromosome 10
97,571.4 Kb
97,572.4 Kb
ER, Vehicle rep1
ER, Vehicle rep2
ER, Vehicle rep3
ER, Vehicle rep4
ER, Decitabine rep1
ER, Decitabine rep2
ER, Decitabine rep3
ER, Decitabine rep4
EPIC, Vehicle rep1
EPIC, Vehicle rep2
EPIC, Vehicle rep3
EPIC, Vehicle rep4
EPIC, Decitabine rep1
EPIC, Decitabine rep2
EPIC, Decitabine rep3
EPIC, Decitabine rep4
CpG site
ERE motif
Active Enhancer
ANKRD2

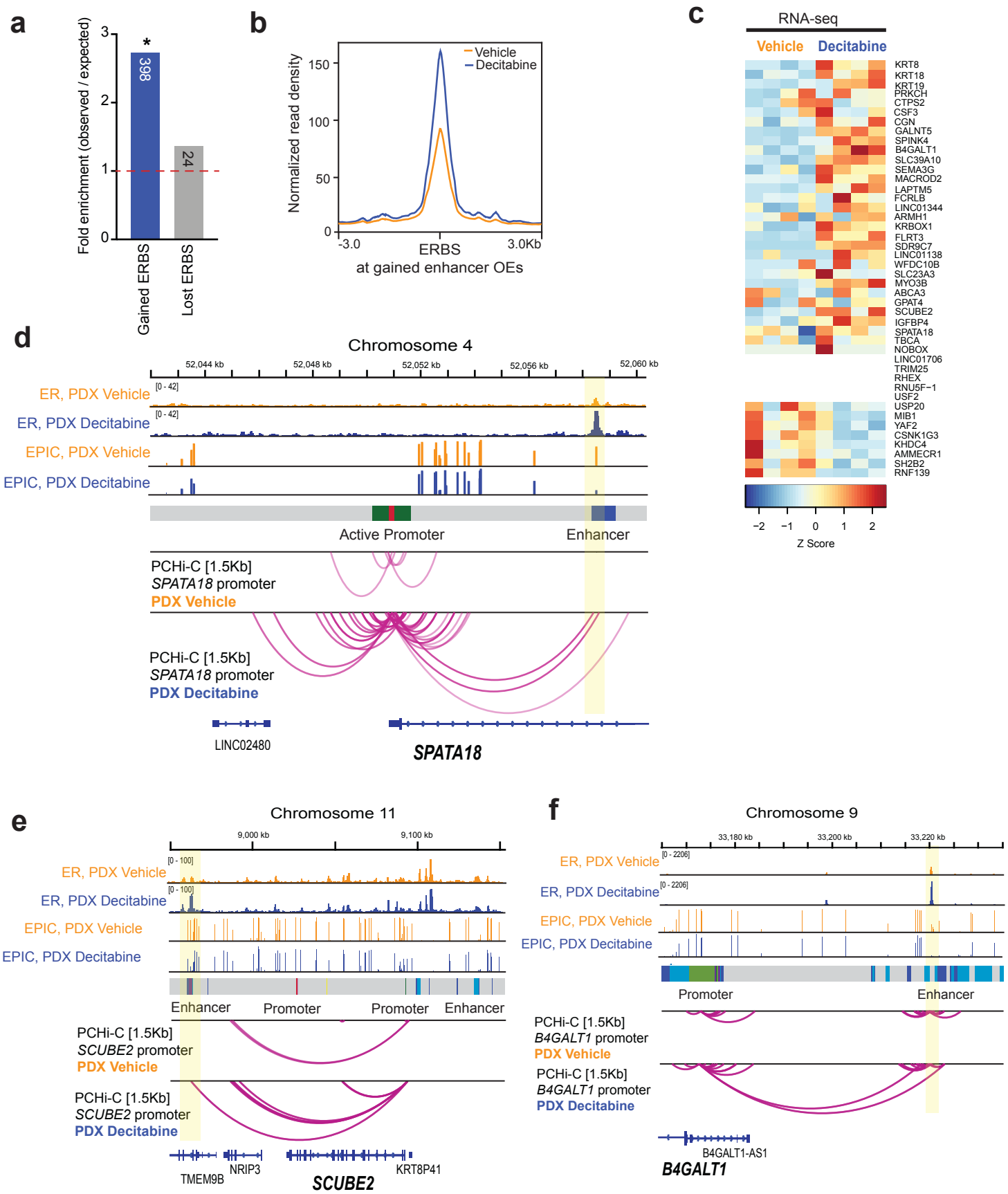
a
Fold enrichment (observed / expected)
398
241
Gained ERBS
Lost ERBS
b
Normalized read density
Vehicle
Decitabine
-3.0
ERBS
3.0Kb
at gained enhancer OEs
c
RNA-seq
Vehicle
Decitabine
Z Score
d
Chromosome 4
52,044 kb
52,048 kb
52,052 kb
52,056 kb
52,060 kb
ER, PDX Vehicle
ER, PDX Decitabine
EPIC, PDX Vehicle
EPIC, PDX Decitabine
Active Promoter
Enhancer
PCHi-C [1.5Kb]
SPATA18 promoter
PDX Vehicle
PCHi-C [1.5Kb]
SPATA18 promoter
PDX Decitabine
LINC02480
SPATA18
e
Chromosome 11
9,000 kb
9,100 kb
ER, PDX Vehicle
ER, PDX Decitabine
EPIC, PDX Vehicle
EPIC, PDX Decitabine
Enhancer
Promoter
Promoter
Enhancer
PCHi-C [1.5Kb]
SCUBE2 promoter
PDX Vehicle
PCHi-C [1.5Kb]
SCUBE2 promoter
PDX Decitabine
TMEM9B
NRIP3
KRT8P41
SCUBE2
f
Chromosome 9
33,180 kb
33,200 kb
33,220 kb
ER, PDX Vehicle
ER, PDX Decitabine
EPIC, PDX Vehicle
EPIC, PDX Decitabine
Promoter
Enhancer
PCHi-C [1.5Kb]
B4GALT1 promoter
PDX Vehicle
PCHi-C [1.5Kb]
B4GALT1 promoter
PDX Decitabine
B4GALT1-AS1
B4GALT1

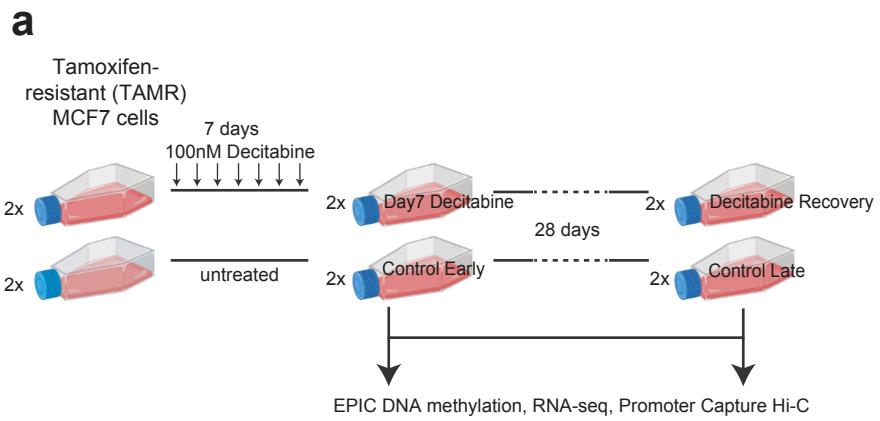
a
Tamoxifen-resistant (TAMR) MCF7 cells
7 days
100nM Decitabine
2x
2x
untreated
2x Day7 Decitabine
2x Decitabine Recovery
28 days
2x Control Early
2x Control Late
EPIC DNA methylation, RNA-seq, Promoter Capture Hi-C

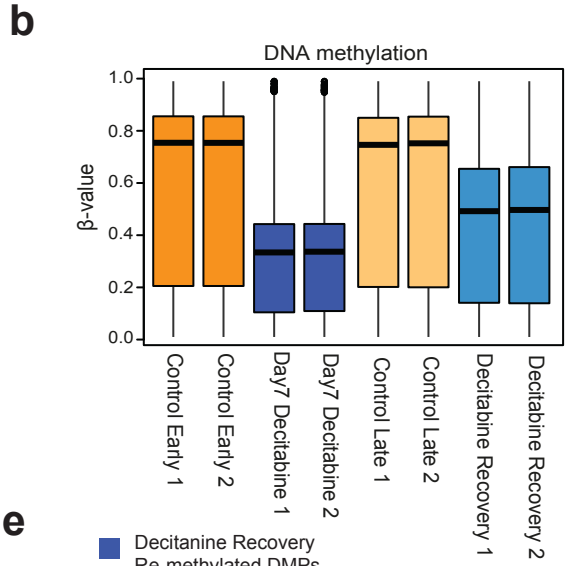
b
DNA methylation
β-value
1.0
0.8
0.6
0.4
0.2
0.0
Control Early 1
Control Early 2
Day7 Decitabine 1
Day7 Decitabine 2
Control Late 1
Control Late 2
Decitabine Recovery 1
Decitabine Recovery 2

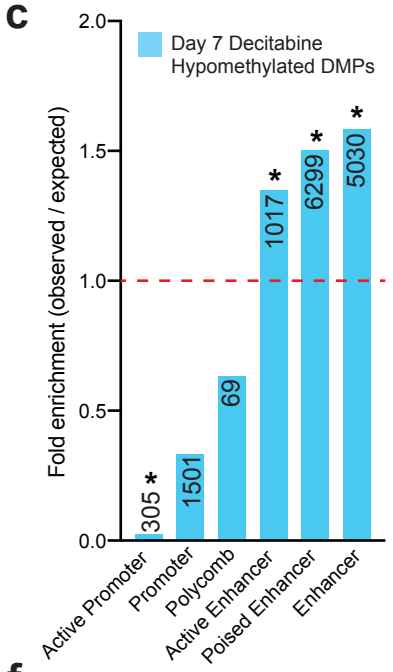
c
Day 7 Decitabine Hypomethylated DMPs
Fold enrichment (observed / expected)
2.0
1.5
1.0
0.5
0.0
305
1501
69
1017
6299
5030
Active Promoter
Promoter
Polycomb
Active Enhancer
Poised Enhancer
Enhancer

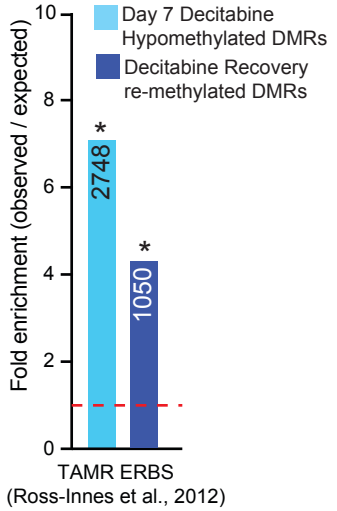
d
Day 7 Decitabine Hypomethylated DMRs
Decitabine Recovery re-methylated DMRs
Fold enrichment (observed / expected)
10
8
6
4
2
0
2748
1050
TAMR ERBS
(Ross-Innes et al., 2012)

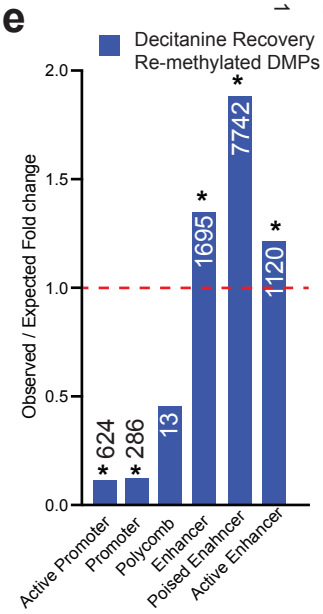
e
Decitanine Recovery Re-methylated DMPs
Observed / Expected Fold change
2.0
1.5
1.0
0.5
0.0
624
286
13
1695
7742
1120
Active Promoter
Promoter
Polycomb
Enhancer
Poised Enhancer
Active Enhancer

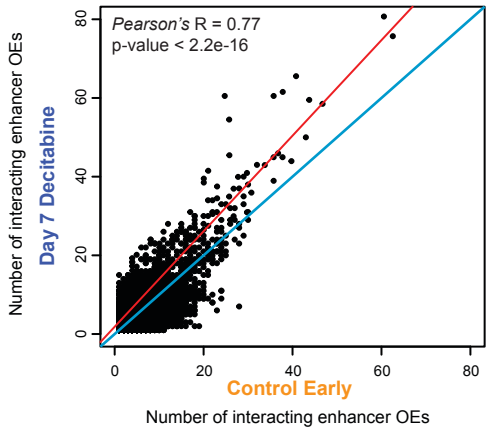
f
Pearson's R = 0.77
p-value < 2.2e-16
Number of interacting enhancer OEs
Day 7 Decitabine
0
20
40
60
80
Control Early
Number of interacting enhancer OEs

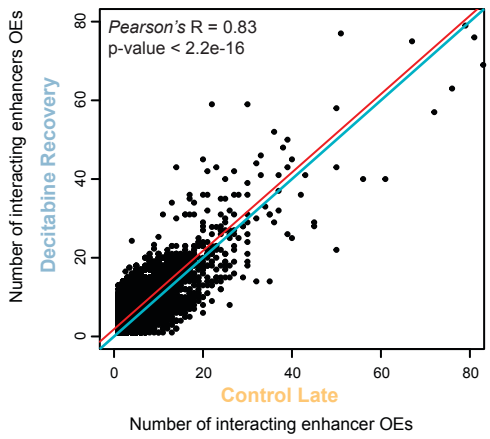
g
Pearson's R = 0.83
p-value < 2.2e-16
Number of interacting enhancers OEs
Decitabine Recovery
0
20
40
60
80
Control Late
Number of interacting enhancer OEs

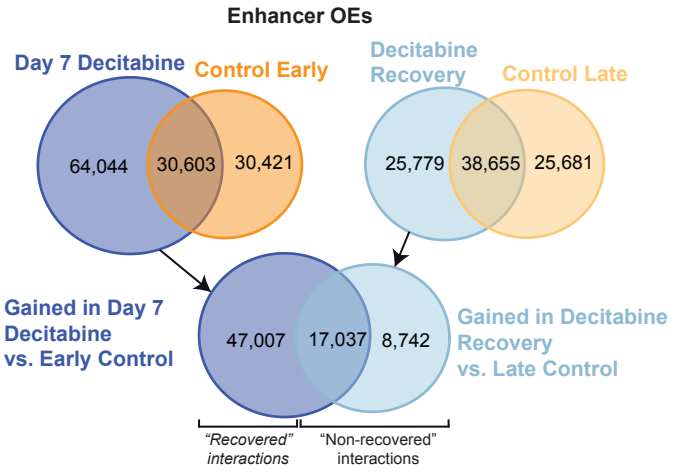
h
Enhancer OEs
Day 7 Decitabine
Control Early
Decitabine Recovery
Control Late
64,044
30,603
30,421
25,779
38,655
25,681
Gained in Day 7 Decitabine vs. Early Control
47,007
17,037
8,742
Gained in Decitabine Recovery vs. Late Control
"Recovered" interactions
"Non-recovered" interactions

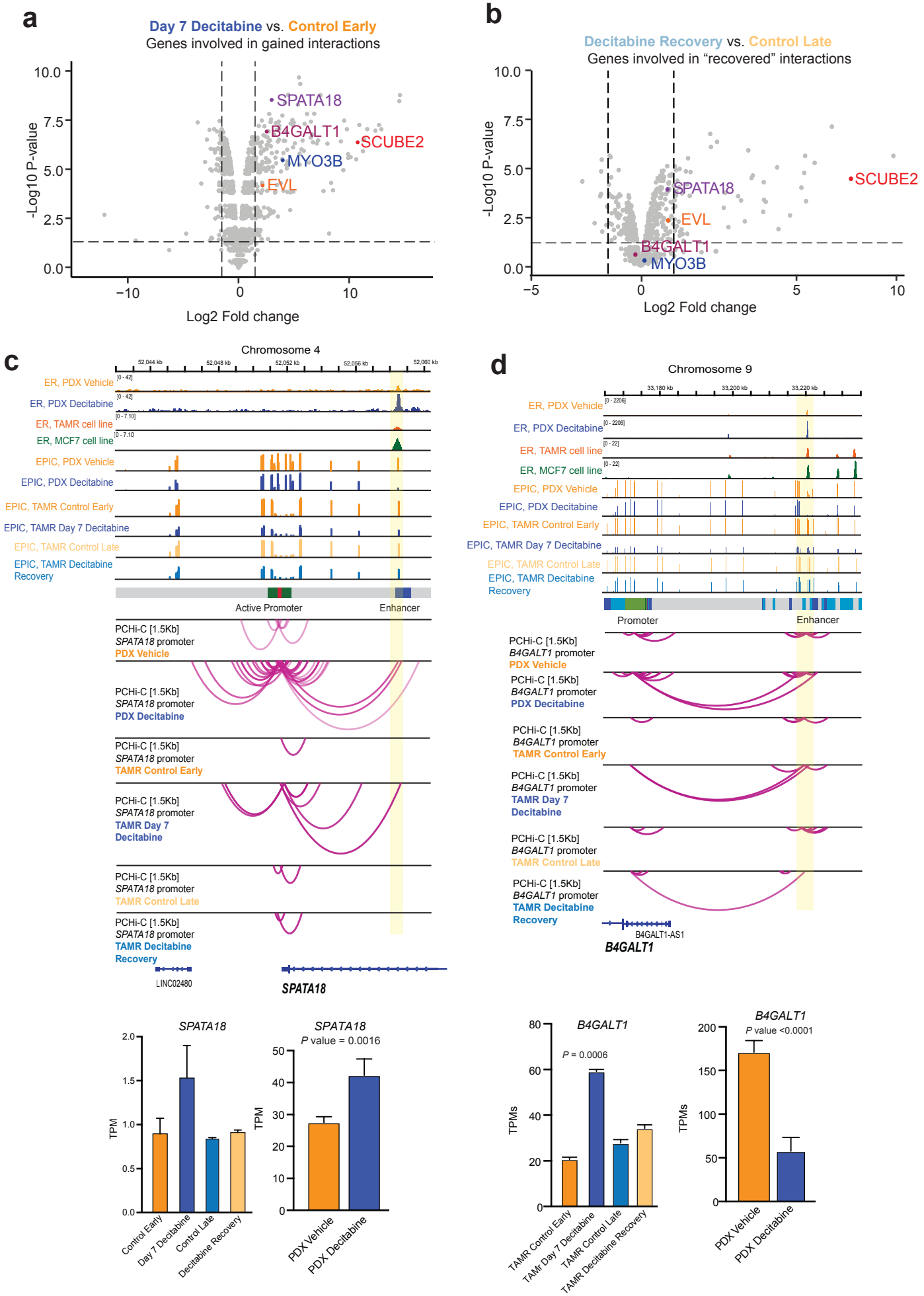
a
Day 7 Decitabine vs. Control Early
Genes involved in gained interactions
-Log10 P-value
Log2 Fold change
SPATA18
B4GALT1
SCUBE2
MYO3B
EVL
b
Decitabine Recovery vs. Control Late
Genes involved in "recovered" interactions
-Log10 P-value
Log2 Fold change
SCUBE2
SPATA18
EVL
B4GALT1
MYO3B
c
Chromosome 4
ER, PDX Vehicle
ER, PDX Decitabine
ER, TAMR cell line
ER, MCF7 cell line
EPIC, PDX Vehicle
EPIC, PDX Decitabine
EPIC, TAMR Control Early
EPIC, TAMR Day 7 Decitabine
EPIC, TAMR Control Late
EPIC, TAMR Decitabine Recovery
Active Promoter
Enhancer
PCHi-C [1.5Kb] SPATA18 promoter PDX Vehicle
PCHi-C [1.5Kb] SPATA18 promoter PDX Decitabine
PCHi-C [1.5Kb] SPATA18 promoter TAMR Control Early
PCHi-C [1.5Kb] SPATA18 promoter TAMR Day 7 Decitabine
PCHi-C [1.5Kb] SPATA18 promoter TAMR Control Late
PCHi-C [1.5Kb] SPATA18 promoter TAMR Decitabine Recovery
LINC02480
SPATA18
d
Chromosome 9
ER, PDX Vehicle
ER, PDX Decitabine
ER, TAMR cell line
ER, MCF7 cell line
EPIC, PDX Vehicle
EPIC, PDX Decitabine
EPIC, TAMR Control Early
EPIC, TAMR Day 7 Decitabine
EPIC, TAMR Control Late
EPIC, TAMR Decitabine Recovery
Promoter
Enhancer
PCHi-C [1.5Kb] B4GALT1 promoter PDX Vehicle
PCHi-C [1.5Kb] B4GALT1 promoter PDX Decitabine
PCHi-C [1.5Kb] B4GALT1 promoter TAMR Control Early
PCHi-C [1.5Kb] B4GALT1 promoter TAMR Day 7 Decitabine
PCHi-C [1.5Kb] B4GALT1 promoter TAMR Control Late
PCHi-C [1.5Kb] B4GALT1 promoter TAMR Decitabine Recovery
B4GALT1-AS1
B4GALT1
SPATA18
TPM
Control Early
Day 7 Decitabine
Control Late
Decitabine Recovery
SPATA18
P value = 0.0016
PDX Vehicle
PDX Decitabine
B4GALT1
P = 0.0006
TPMs
TAMR Control Early
TAMr Day 7 Decitabine
TAMR Control Late
TAMR Decitabine Recovery
B4GALT1
P value <0.0001
PDX Vehicle
PDX Decitabine

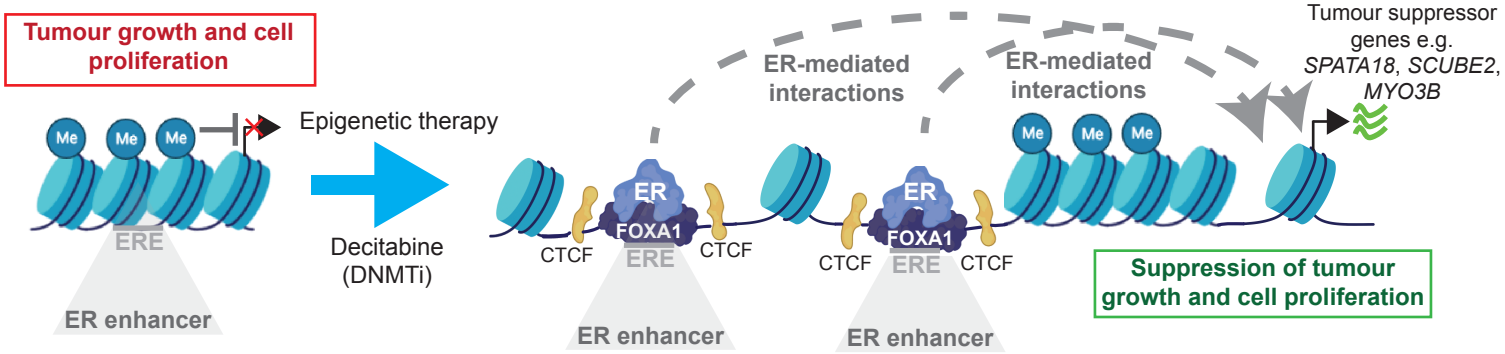
Tumour growth and cell proliferation
Me
Me
Me
ERE
ER enhancer
Epigenetic therapy
Decitabine
(DNMTi)
ER
FOXA1
CTCF
ERE
CTCF
ER enhancer
ER-mediated interactions
ER
FOXA1
CTCF
ERE
CTCF
ER enhancer
ER-mediated interactions
Me
Me
Me
Tumour suppressor genes e.g.
SPATA18, SCUBE2, MYO3B
Suppression of tumour growth and cell proliferation